

Accepted Manuscript

Carbazole-based small molecules for vacuum-deposited organic photovoltaic devices with open-circuit voltage exceeding 1 V

Yuan Jay Chang, Jung-Lien Hsu, Yi-Hua Li, Sajal Biring, Tzu-Hung Yeh, Jhih-Yan Guo, Shun-Wei Liu



PII: S1566-1199(17)30198-2

DOI: [10.1016/j.orgel.2017.05.007](https://doi.org/10.1016/j.orgel.2017.05.007)

Reference: ORGELE 4078

To appear in: *Organic Electronics*

Received Date: 14 February 2017

Revised Date: 12 April 2017

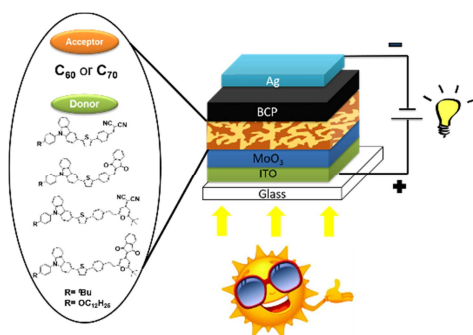
Accepted Date: 4 May 2017

Please cite this article as: Y.J. Chang, J.-L. Hsu, Y.-H. Li, S. Biring, T.-H. Yeh, J.-Y. Guo, S.-W. Liu, Carbazole-based small molecules for vacuum-deposited organic photovoltaic devices with open-circuit voltage exceeding 1 V, *Organic Electronics* (2017), doi: 10.1016/j.orgel.2017.05.007.

This is a PDF file of an unedited manuscript that has been accepted for publication. As a service to our customers we are providing this early version of the manuscript. The manuscript will undergo copyediting, typesetting, and review of the resulting proof before it is published in its final form. Please note that during the production process errors may be discovered which could affect the content, and all legal disclaimers that apply to the journal pertain.

Graphical Abstract

Carbazole-based p-type donor molecules for vacuum-deposited organic photovoltaic devices exhibited the open-circuit voltage exceeding 1 V



Carbazole-based small molecules for vacuum-deposited organic photovoltaic devices with open-circuit voltage exceeding 1 V

Yuan Jay Chang^{a,*}, Jung-Lien Hsu^a, Yi-Hua Li^b, Sajal Biring^b, Tzu-Hung Yeh^{b,c}, Jihh-Yan Guo^b, and Shun-Wei Liu^{b,*}

^a*Department of Chemistry, Tunghai University, Taichung 40704, Taiwan*

^b*Department of Electronic Engineering and Organic Electronics Research Center, Ming Chi University of Technology, New Taipei City 24301, Taiwan*

^c*Department of Electronic Engineering, National Taiwan University of Science and Technology, Taipei 10607, Taiwan*

*Corresponding author.

E-mail address: jaychang@thu.edu.tw (Y. J. Chang) and swliu@mail.mcut.edu.tw (S. -W. Liu)

Abstract

Fabrication of vacuum deposited small molecules organic solar cell with open-circuit voltage (V_{oc}) exceeding 1V is crucial in advancing the applications of organic photovoltaics (OPVs). Here, a novel carbazole-based donor- π bridge-acceptor (D- π -A) of p-type material (F-series) in combination with fullerene derivative C₆₀ or C₇₀ as n-type material for bulk-heterojunction OPVs with the structure of ITO/ MoO₃ (15 nm)/ F-series donor: C₆₀ or C₇₀ (40 or 80 nm)/BCP (7 nm)/ Ag (120 nm) have been proposed. The vacuum deposited small molecules OPV with the donor layer consisting of F1 combined with the electron acceptor C70 exhibits a high power conversion efficiency (PCE) of 4.93%. The higher PCE of the OPV is attributed to the large VOC value of 1.02 V. The analysis of photophysical properties using a time-dependent density functional theory model and the B3LYP functional corroborates the experimental results and provides the evidence on increasing the V_{oc} of OPVs.

Keywords: Organic photovoltaics, small-molecule organic solar cells, planar mixed heterojunction, highly open-circuit voltage

1. Introduction

The global energy demand is raised rapidly in current year [1-2]. Combustion of fossil fuels produces large quantities of greenhouse gases, which may have catastrophic consequences resulting in global warming. Therefore, there is an urge to investigate and develop renewable and environmental friendly energy source. Especially solar energy has tremendous potential as alternative energy resource. In the past two decades, compared with silicon-based photovoltaic devices, the organic photovoltaics (OPVs) have received considerable attention due to its ease of fabrication, extended absorption range by tuning structure, colorful transparency, compatibility with flexible substrates, large area processing, and low fabrication cost of device [3-5]. A general notion in OPVs research field regarding the successful improvement of power conversion efficiency (PCE) is to use a p-type conjugated polymer as a donor and the fullerene derivative PC61BM as an acceptor. Currently, PCE of polymer-based solar cells have been reached over 10% using solution processed bulk-heterojunction (BHJ) with tandem cell structure [6-8].

The small molecules can receive the predominant advantages over the polymeric materials having well-defined molecular structures, easier purification, higher reliability and better reproducibility. Therefore, enormous research works have been carried out with small-molecule OPVs, which exhibit appreciable PCEs of $> 6\%$ using vacuum-deposition fabrication techniques [9-11]. Although, in general, the solution processing is considered to be more cost-effective compared to vacuum deposition, but solution processing creates leakage paths between anode and cathode due to either p-type or n-type phase continuity arising from spin-coating of the solvent to form the film [12-13]. On the other hand, vacuum deposition technique of OPVs shows higher

potential availing the advantage of easy fabrication of multilayered tandem architectures. Of late, a tandem cell of OPV device with a PCE of up to 11% has been reported [14].

Recently, researches on new small molecule-based p-type material in OPVs have developed a large variety of promising organic materials with different donor-acceptor moiety combinations. For example, symmetrical acceptor-donor-acceptor (A-D-A), [15-19] donor-acceptor-donor (D-A-D), [20-22] unsymmetrical D-A, [23-25] and D-A-A' [9-10, 26-27] systems have been synthesized with PCE approaching those of polymeric system. A wide variety of prominent chemical structures of photovoltaic materials with vacuum processed deposition have been reported in the literatures including the oligothiophene, [15, 28-29] phthalocyanines (Pc), [30] subphthalocyanines (SubPc), [31-34] squaraine, [35-37] and triarylamine [38-40].

Although the device performance is improved continuously by using unique property of materials and fabrication architectures of device, but it is still inadequate in meeting commercial requirements [41-42]. The previous reports have focused on the panchromatic absorption range and photocurrent output using various active materials [38, 43-45] and device structures [46-48]. However, one of the crucial limitations for device performance is the low value of open-circuit voltage (V_{oc}). Carbazole structure possesses weak electron donating ability which is one of crucial factors for designing higher HOMO energy level of p-type material in order to achieve high V_{oc} value in organic photovoltaics devices.

To date, most of the previous publications have reported V_{oc} value in solution processed devices using the symmetry structure based on carbazole core as p-type or n-type materials [49-54]. In this work, we have used carbazole as electron donating moiety with four acceptors applying D- π -A dipolar system as p-type material in photovoltaic solar cells. We have fabricated a highly efficient OPVs device with ITO/MoO₃/Active layer/ BCP/Ag by vacuum deposition technique. The active layer

consisting of **F1** combined with the electron acceptor C₇₀ exhibits a high PCE of 4.93%, which is attributed to the higher V_{oc} value of 1.02 V.

2. Experimental Section

2.1 General Information

All reactions and manipulations were performed in a nitrogen atmosphere. Solvents were distilled freshly according to standard procedures. ¹H and ¹³C NMR spectra were recorded on a Bruker (AV 400/AVIII HD 400/AV 500 MHz) spectrometer, and CDCl₃ was used as solvents. Chemical shifts were reported on the δ scale downfield from the tetramethylsilane peak. Absorption spectra were recorded on a SHIMADZU UV-1800 and Jasco V-630 spectrophotometer, and emission spectra were obtained using a Hitachi F-4500 spectrofluorimeter. Emission spectra in solutions were measured using a spectral grade solvent and right-angle detection. For material analysis, the photoelectron spectrometer (AC-2, Riken Keiki) was used to measure the ITO work function and the HOMO level of the organic materials. Mass spectra were recorded on a JEOL JMS-700 double-focusing mass spectrometer. The surface morphology of the materials was characterized by the non-contact mode atomic force microscopy (AFM). Thermogravimetric analysis (TGA; Pyris 1 TGA Lab system) measurements were carried out with heating rate of 10 °C/min under a nitrogen gas atmosphere.

The chemicals *N*-Bromosuccinimide (NBS), *trans*-Dichlorobis(triphenylphosphine) palladium(II) (PdCl₂(PPh₃)₂), 2-(Tributyl-stannyl)thiophene, *n*-Butyllithium (1.6 M in hexane), *N,N'*-Dimethylformamide, 4-Bromobenzaldehyde, tri-*n*-Butyltin chloride, Malononitrile, 1,3-Indandione, Ammonium acetate, and Piperidine were purchased from Acros, Alfa, Merck, Lancaster, TCI, Sigma-Aldrich, and Showa, separately, and purified when necessary. Chromatographic separations were performed using silica gel from Merck (Kieselgel Si 60; 40–63 μ m).

2.2 Fabrication and Characterization of Bulk-Heterojunction OPVs

Devices were fabricated as described using the basic method described in our previous work [34, 55]. The bulk-heterojunction OPVs devices was consisted of F-series organic dyes and fullerene derivative C₆₀ or C₇₀ as the p-type and n-type materials, MoO₃ as hole transporting material, and BCP as the buffer between the n-type material and the cathode. All materials were purified by sublimation before use. The patterned indium-tin-oxide (ITO) substrates as the anode with a sheet resistance of 10 Ω/sq were purchased from Lumtec. The ITO substrates were cleaned by detergent, deionized water, acetone, and isopropanol in sequence, and subsequently the substrates were transferred to a vacuum chamber of the thermal evaporator, and the organic active materials were deposited in the sequence of ITO/ MoO₃ (15 nm)/ F-series donor:C₆₀ or C₇₀ (40 or 80 nm)/BCP (7 nm)/ Ag (120 nm) under the pressure of 6*10⁻⁶ Torr. The constant deposition rates of MoO₃ was 0.03 nm/s, and the other organic materials were controlled within 0.1~0.2 nm/s. A cathode material of Ag was deposited in the chamber through a shadow mask to define active regions of the devices (4 mm²) by the overlapping area between ITO/organic layer/Ag. After the evaporation, the devices were transferred to a grove box and go encapsulation process under the N₂ environment to prevent damage from the oxygen and moisture.

The *J-V* characteristics of the OPVs devices were measured with a current source meter (Keithley 2400) under dark conditions and under the illumination of a 1-sun AM 1.5G solar simulator (91160, Newport), which was calibrated through a Si reference cell. For measuring the external quantum efficiency (EQE) spectra, the AM 1.5G solar simulator was used to generate the bias light. A monochromator, which was calibrated with a photodiode and chopped at 250 Hz, was used to select wavelengths between 350 and 800 nm to illuminate the OPVs. The photocurrent of the OPVs was measured through the lock-in amplifier, which was referenced to the chopper frequency. After

measuring the devices, the results of the EQE spectra were integrated to obtain the J_{sc} of the devices and were subsequently compared with the J_{sc} , which were measured under illumination of the solar simulator.

2.3 Synthesis of dyes

The structures of carbazole-based organic dyes and their synthetic sequences are presented in Fig. 1 and Scheme 1.

2.3.1 9-(4-*tert*-Butylphenyl)-3-bromo-9H-carbazole (**2a**).

A mixture of **1a** (4.9 g, 16.38 mmol) in dry CH_2Cl_2 was placed in a three-necked flask under a nitrogen atmosphere. Following this, added dropwise NBS (2.91 g, 16.38 mmol) in CH_2Cl_2 to this reaction and stirred 6 hours room temperature. The mixture was quenched by adding DI water, and the mixture extracted with CH_2Cl_2 . The organic layer was dried over anhydrous MgSO_4 and evaporated under vacuum. The product was purified by silica gel column chromatograph with hexane as eluent. White solid of **2a** was obtained in 78% yield (4.81 g, 12.77 mmol). ^1H NMR (400 MHz, CDCl_3): δ 8.28 (s, 1H), 8.11 (d, 1H, $J = 8.0$ Hz), 7.63 (d, 2H, $J = 8.4$ Hz), 7.51-7.44 (m, 5H), 7.33-7.30 (m, 2H), 1.46 (s, 9H). ^{13}C NMR (100 MHz, CDCl_3): δ 150.8, 141.3, 139.6, 134.4, 128.4, 126.8, 126.6, 126.5, 124.9, 122.9, 122.1, 120.4, 120.1, 112.4, 111.4, 110.1, 34.8, 31.4. MS (FAB, 70 eV): m/z (relative intensity) 377 (M^+ , 100); HRMS calcd for $\text{C}_{22}\text{H}_{20}\text{N}^{79}\text{Br}$: 377.0779, found 377.0773.

2.3.2 3-Bromo-9-(4-(dodecyloxy)phenyl)-9H-carbazole (**2b**).

Compound **2b** was synthesized according to the same procedure as that of **2a**. Yellow solid was obtained in 50% yield. ^1H NMR (400 MHz, CDCl_3): δ 8.26 (s, 1H), 8.10 (d, 1H, $J = 7.72$ Hz), 7.44-7.50 (m, 4 H), 7.41 (d, 2H, $J = 8.68$ Hz), 7.33 (d, 1H, $J = 8.44$ Hz), 7.29 (d, 1H, $J = 7.76$ Hz), 7.21 (d, 1H, $J = 8.64$ Hz), 7.12 (d, 2H, $J = 8.76$ Hz),

4.07 (t, 2H, $J = 6.48$ Hz), 1.84-1.90 (m, 2 H), 1.50-1.56 (m, 2 H), 1.32-1.44 (m, 16 H), 0.92 (t, 3H, $J = 6.96$ Hz); ^{13}C NMR (100 MHz, CDCl_3): δ 158.7, 141.7, 140.0, 129.5, 128.5, 128.4, 126.5, 124.8, 122.9, 122.0, 120.4, 120.0, 115.6, 112.3, 111.2, 109.9, 68.4, 31.9, 29.7, 29.6, 29.4, 29.3, 29.2, 26.0, 22.7, 14.1. MS (FAB, 70 eV): m/z (relative intensity) 505 (M^+ , 100); HRMS calcd for $\text{C}_{30}\text{H}_{36}\text{BrNO}$: 505.1975, found 505.1958.

2.3.3 9-(4-*tert*-Butylphenyl)-3-(thiophen-2-yl)-9H-carbazole (**3a**).

To a three-necked flask containing a mixture of **2a** (4.5 g, 11.93 mmol), $\text{PdCl}_2(\text{PPh}_3)_2$ (0.26 g, 0.36 mmol), 2-tributylstannylthiophene (10.2 mL, 27.44 mmol) was added DMF (30 mL). The reaction mixture was stirred at 90 °C for 24 h. After cooling, the reaction was quenched by adding methanol and $\text{KF}_{(\text{aq})}$ (saturated 45 mL). The mixture was extracted with CH_2Cl_2 and the organic layer dried over anhydrous MgSO_4 . Evaporation of the solvent gave the crude, which was purified by silica gel with CH_2Cl_2 /hexane (1/3) as eluent. Yellow solid of **3a** was obtained in 82% (3.73 g, 9.78 mmol). ^1H NMR (400 MHz, CDCl_3): δ 8.38 (s, 1H), 8.20 (d, 1H, $J = 7.6$ Hz), 7.69 (d, 1H, $J = 8.8$ Hz), 7.64 (d, 2H, $J = 8.4$ Hz), 7.51 (d, 2H, $J = 8.4$ Hz), 7.45-7.42 (m, 3H), 7.41 (d, 1H, $J = 3.6$ Hz), 7.34-7.28 (m, 2H), 7.14 (t, 1H, $J = 4.0$ Hz), 1.46 (s, 9H). ^{13}C NMR (100 MHz, CDCl_3): δ 150.6, 145.6, 141.5, 140.5, 134.7, 127.9, 126.7, 126.6, 126.5, 126.1, 124.5, 123.7, 123.7, 123.1, 122.2, 120.4, 119.9, 117.7, 110.2, 110.1, 34.8, 31.4. MS (FAB, 70 eV): m/z (relative intensity) 381 (M^+ , 100); HRMS calcd for $\text{C}_{26}\text{H}_{23}\text{NS}$: 381.1551, found 381.1554.

2.3.4 9-(4-(Dodecyloxy)phenyl)-3-(thiophen-2-yl)-9H-carbazole (**3b**)

Compound **3b** was synthesized according to the same procedure as that of **3a**. Green solid of **3b** was obtained in 80% yield. ^1H NMR (400 MHz, CDCl_3): δ 8.38 (s, 1H), 7.69 (dd, 1H, $J = 8.52, 1.52$ Hz), 7.42-7.47 (m, 3 H), 7.31-7.38 (m, 4 H), 7.28 (d, 1H, $J = 6.24$ Hz), 7.12-7.15 (m, 3 H), 4.08 (t, 2H, $J = 6.48$ Hz), 1.87-1.90 (m, 2 H), 1.50-1.55

(m, 2 H), 1.32-1.43 (m, 16 H), 0.92 (t, 3H, $J = 6.92$ Hz); ^{13}C NMR (100 MHz, CDCl_3): δ 158.5, 145.7, 141.9, 140.9, 129.8, 128.4, 127.9, 126.5, 126.1, 124.5, 123.7, 123.5, 123.0, 122.1, 120.4, 119.8, 117.7, 115.6, 110.0, 109.9, 68.4, 31.9, 29.6, 29.4, 29.3, 29.2, 26.1, 22.7, 14.1. MS (FAB, 70 eV): m/z (relative intensity) 509 (M^+ , 100); HRMS calcd for $\text{C}_{34}\text{H}_{39}\text{NOS}$: 509.2747, found 509.2751.

2.3.5 4-(5-(9-(4-*tert*-Butylphenyl)-9H-carbazol-3-yl)thiophen-2-yl)benzaldehyde (**4a**).

A mixture of **3a** (2.5 g, 6.56 mmol) was added dropwise BuLi (6.2 mL, 9.84 mmol, 1.6 M in hexane) in dry THF at -78 °C in a three-necked flask under a nitrogen atmosphere. After then the solution was cooled to -40 °C and was stirred by a magnetic bar for 30 minutes. The solution was cooled again to -78 °C and to it was added tri-*n*-butyltin chloride (1.7 mL, 9.84 mmol). The reaction was warmed up to room temperature and stirred overnight. The reaction mixture was quenched by the addition of water, and was extracted with CH_2Cl_2 . The combined organic solution was dried over anhydrous MgSO_4 , and dried under vacuum. The crude product was dissolved in dry DMF, then to it was added 4-bromobenzaldehyde (1.21 g, 6.56 mmol) and $\text{PdCl}_2(\text{PPh}_3)_2$ (148 mg, 0.2 mmol). The solution was heated to 90 °C for 24 h and then cooled. The reaction was quenched by the addition of methanol and saturated $\text{KF}_{(\text{aq})}$ (15 mL). The mixture was extracted with CH_2Cl_2 , while the organic layer was dried over anhydrous MgSO_4 . Evaporation of the solvent gave a crude product, which was purified by silica gel column chromatograph eluted by $\text{CH}_2\text{Cl}_2/\text{hexane}$ (1/1). Yellow solid of **4a** was obtained in 75% yield. ^1H NMR (400 MHz, CDCl_3): δ 10.02 (s, 1H), 8.42 (s, 1H), 8.21 (d, 1H, $J=7.6$ Hz), 7.92 (d, 2H, $J=8.4$ Hz), 7.83 (d, 2H, $J=8.4$ Hz), 7.71 (d, 1H, $J=8.4$ Hz), 7.65 (d, 2H, $J=8.4$ Hz), 7.52-7.44 (m, 6H), 7.41 (d, 1H, $J=3.6$ Hz), 7.36-7.32 (m, 1H), 1.46 (s, 9H). ^{13}C NMR (100 MHz, CDCl_3): δ 191.4, 150.7, 147.4, 141.6, 140.8, 140.5, 140.3, 134.8, 134.5, 130.5, 126.8, 126.5, 126.3, 126.1, 125.9, 125.4, 124.1, 123.8, 123.4, 123.0, 120.4, 120.1, 117.6, 110.4, 110.2, 34.8, 31.4. MS (FAB, 70 eV): m/z

(relative intensity) 485 (M^+ , 100); HRMS calcd for $C_{33}H_{27}NOS$: 485.1813, found 485.1814.

2.3.6 *4-(5-(9-(4-(Dodecyloxy)phenyl)-9H-carbazol-3-yl)thiophen-2-yl)benzaldehyde (4b).*

Compound **4b** was synthesized according to the same procedure as that of **4a**. Yellow solid of **4b** was obtained in 71% yield. 1H NMR (400 MHz, $CDCl_3$): δ 9.99 (s, 1H), 8.38 (s, 1H), 8.17 (d, 1H, $J = 7.68$ Hz), 7.89 (d, 2H, $J = 8.12$ Hz), 7.79 (d, 2H, $J = 8.2$ Hz), 7.58 (dd, 1H, $J = 8.56, 1.48$ Hz), 7.47 (d, 1H, $J = 3.8$ Hz), 7.41-7.44 (m, 3H), 7.36 (d, 1H, $J = 3.8$ Hz), 7.28-7.34 (m, 3H), 7.10 (d, 2H, $J = 8.72$ Hz), 4.06 (d, 2H, $J = 6.52$ Hz), 1.84-1.87 (m, 2H), 1.48-1.53 (m, 2H), 1.28-1.39 (m, 16H), 0.88 (d, 3H, $J = 6.08$ Hz); ^{13}C NMR (100 MHz, $CDCl_3$): δ 191.3, 158.7, 147.5, 142.0, 141.2, 140.5, 140.3, 134.8, 130.4, 129.6, 128.4, 126.3, 126.1, 125.8, 125.4, 124.2, 123.6, 123.4, 122.9, 120.3, 120.0, 117.6, 115.6, 110.2, 110.0, 68.4, 31.9, 29.6, 29.4, 29.3, 29.2, 26.0, 22.6, 14.0; MS (FAB, 70 eV): m/z (relative intensity) 613 (M^+ , 100); HRMS calcd for $C_{41}H_{43}NO_2S$: 613.3009, found 613.2998.

2.3.7 *2-((4-(5-(9-(4-tert-Butylphenyl)-9H-carbazol-3-yl)thiophen-2-yl)phenyl)-methylene)malononitrile (F1).*

A mixture of **4a** (1.8 g, 3.71 mmol), and malononitrile (0.28 mL, 4.45 mmol) were placed in a three-necked flask containing dry THF (20 mL) under N_2 . The resulted mixture was heated to reflux for 24 hours. After cooling, the reaction was quenched by pouring into water and it was extracted with CH_2Cl_2 . The combined organic layer was dried over anhydrous $MgSO_4$ and evaporated under vacuum. The mixture was purified by silica gel column chromatograph with CH_2Cl_2 as eluent. The red solid of **F1** was

collected in 80% yield (1.58 g, 2.96 mmol). MP: 145-147 °C. ¹H NMR (400 MHz, CDCl₃): δ 8.34 (d, 1H, *J* = 1.48 Hz), 8.16 (d, 1H, *J* = 7.72 Hz), 7.85 (d, 2H, *J* = 8.52 Hz), 7.72 (d, 2H, *J* = 8.52 Hz), 7.65 (dd, 1H, *J* = 8.52, 1.84 Hz), 7.59-7.61 (m, 3H), 7.38-7.48 (m, 6H), 7.35 (d, 1H, *J* = 3.84 Hz), 7.28-7.32 (m, 1H), 1.42 (s, 9H); ¹³C NMR (100 MHz, CDCl₃): δ 158.4, 150.8, 148.8, 141.6, 140.9, 140.5, 139.8, 134.4, 131.6, 129.2, 126.9, 126.8, 126.4, 125.5, 124.1, 123.8, 123.6, 123.0, 120.3, 120.2, 117.6, 114.1, 113.0, 110.4, 110.2, 80.6, 34.8, 31.4; MS (FAB, 70 eV): *m/z* (relative intensity) 533 (M⁺, 100); HRMS calcd for C₃₆H₂₇N₃S: 533.1920, found 533.1911.

2.3.8 2-((4-(5-(9-(4-*tert*-Butylphenyl)-9*H*-carbazol-3-yl)thiophen-2-yl)phenyl)-methylene)-2*H*-indene-1,3-dione (**F2**).

Compound **F2** was synthesized according to the same procedure as that of **F1**. Red solid of **F2** was obtained in 76% yield. MP: 176-178 °C. ¹H NMR (400 MHz, CDCl₃): δ 8.53 (d, 2H, *J* = 8.36 Hz), 8.38 (d, 1H, *J* = 1.44 Hz), 8.20 (d, 1H, *J* = 7.88 Hz), 7.98-8.03 (m, 2H), 7.86 (s, 1H), 7.77-7.80 (m, 4H), 7.64 (d, 2H, *J* = 8.52 Hz), 7.49-8.7.52 (m, 3H), 7.42-7.45 (m, 3H), 7.38 (d, 1H, *J* = 3.92 Hz), 7.31-7.35 (m, 1H), 1.46 (s, 9H); ¹³C NMR (100 MHz, CDCl₃): δ 190.4, 189.1, 150.7, 147.4, 146.0, 142.5, 141.6, 141.0, 140.8, 140.0, 139.1, 135.2, 135.1, 134.9, 134.6, 131.9, 128.3, 126.8, 126.5, 126.3, 126.2, 126.0, 125.1, 124.1, 123.9, 123.8, 123.5, 123.2, 123.1, 120.4, 120.1, 117.6, 110.3, 110.1, 34.8, 31.4. MS (FAB, 70 eV): *m/z* (relative intensity) 613 (M⁺, 100); HRMS calcd for C₄₂H₃₁NO₂S: 613.2076, found 613.2083.

2.3.9 2-(2-*tert*-Butyl-6-((*E*)-2-(4-(5-(9-(4-*tert*-butylphenyl)-9*H*-carbazol-3-yl)-thiophen-2-yl)phenyl)vinyl)-4*H*-pyran-4-ylidene)malononitrile (**F3**).

A mixture of **4a** (1.8 g, 3.71 mmol), 2-(2-*tert*-Butyl-6-methyl-4*H*-pyran-4-ylidene)-malononitrile (794 mg, 3.71 mmol), and piperidine (0.41 mL, 4.08 mmol) were placed

in a three-necked flask containing dry acetonitrile (20 mL) under N₂. The resulted mixture was heated to reflux for 24 hours. After cooling, the reaction was quenched by pouring into water and it was extracted with CH₂Cl₂. The combined organic layer was dried over anhydrous MgSO₄ and evaporated under vacuum. The mixture was purified by silica gel column chromatograph with CH₂Cl₂ as eluent. The red solid of **F3** was collected in 60% yield (1.51 g, 2.23 mmol). MP: 145-147 °C. ¹H NMR (500 MHz, CDCl₃): δ 8.37 (d, 1H, *J* = 1.35 Hz), 8.16 (d, 1H, *J* = 7.70 Hz), 7.69 (d, 2H, *J* = 8.30 Hz), 7.66 (dd, 1H, *J* = 8.55, 1.55 Hz), 7.60 (d, 2H, *J* = 8.40 Hz), 7.55 (d, 2H, *J* = 8.30 Hz), 7.47 (d, 2H, *J* = 8.35 Hz), 7.40-7.41 (m, 4H), 7.28-7.37 (m, 3H), 6.72 (d, 1H, *J* = 15.90 Hz), 6.69 (d, 1H, *J* = 1.80 Hz), 6.55 (d, dH, *J* = 1.90 Hz), 1.42 (s, 9H), 1.38 (s, 9H); ¹³C NMR (125 MHz, CDCl₃): δ 172.1, 158.8, 156.5, 150.7, 146.3, 141.6, 141.1, 140.7, 137.1, 136.5, 134.6, 133.1, 128.5, 126.8, 126.5, 126.3, 126.1, 125.7, 125.1, 124.1, 123.8, 123.3, 123.0, 120.4, 120.1, 117.9, 117.5, 115.2, 110.3, 110.2, 107.2, 102.6, 36.7, 34.8, 31.4, 28.1; MS (FAB, 70 eV): *m/z* (relative intensity) 681 (M⁺, 100); HRMS calcd for C₄₆H₃₉N₃OS: 681.2814, found 681.2819.

2.3.10 2-(2-tert-Butyl-6-((E)-2-(4-(5-(9-(4-tert-butylphenyl)-9H-carbazol-3-yl)-thiophen-2-yl)phenyl)vinyl)-4H-pyran-4-ylidene)-2H-indene-1,3-dione (F4).

Compound **F4** was synthesized according to the same procedure as that of **F3**. Orange solid of **F4** was obtained in 66% yield. MP: 176-178 °C. ¹H NMR (500 MHz, CDCl₃): δ 8.44 (s, 1H), 8.40 (s, 1H), 8.35 (d, 1H), 8.14 (d, 1H, *J* = 7.75 Hz), 7.73 (dt, 2H, *J* = 18.7, 3.3 Hz), 7.64-7.67 (m, 3H), 7.53-7.60 (m, 6H), 7.45 (d, 2H, *J* = 8.35 Hz), 7.39-7.39 (m, 3H), 7.36 (d, 2H, *J* = 8.60 Hz), 7.32 (d, 1H, *J* = 3.70 Hz), 7.25-7.28 (m, 1H), 6.85 (d, 1H, *J* = 15.95 Hz), 1.41 (s, 9H), 1.40 (s, 9H); ¹³C NMR (125 MHz, CDCl₃): δ 192.7, 173.8, 160.8, 150.6, 149.2, 146.0, 141.5, 141.3, 140.7, 140.6, 136.0, 135.5, 134.6, 133.6, 133.2, 133.1, 128.3, 126.7, 126.4, 126.2, 126.1, 125.6, 124.8, 124.1,

123.7, 123.2, 123.0, 121.3, 121.2, 120.3, 120.0, 119.6, 117.4, 110.3, 110.1, 109.0, 108.7, 103.5, 36.9, 34.8, 31.4, 28.3. MS (FAB, 70 eV): m/z (relative intensity) 761 (M^+ , 100); HRMS calcd for $C_{52}H_{43}NO_3S$: 761.2964, found 761.2964.

2.3.11 2-((4-(5-(9-(4-(Dodecyloxy)phenyl)-9H-carbazol-3-yl)thiophen-2-yl)-phenyl)methylene)malononitrile (**F5**).

Compound **F5** was synthesized according to the same procedure as that of **F1**. Red solid of **F5** was collected in 80% yield. MP: 145-147 °C. 1H NMR (500 MHz, $CDCl_3$): δ 8.35 (s, 1H), 8.14 (d, 1H, $J = 7.70$ Hz), 7.88 (d, 2H, $J = 8.45$ Hz), 7.73 (d, 2H, $J = 8.40$ Hz), 7.64-7.66 (m, 3H), 7.48 (d, 1H, $J = 3.85$ Hz), 7.39-7.41 (m, 3H), 7.35 (d, 1H, $J = 3.85$ Hz), 7.27-7.31 (m, 3H), 7.08 (d, 2H, $J = 8.70$ Hz), 4.03 (t, 2H, $J = 6.50$ Hz), 1.81-1.84 (m, 2H), 1.47-1.51 (m, 2H), 1.22-1.38 (m, 16H), 0.86 (t, 3H, $J = 7.05$ Hz); ^{13}C NMR (125 MHz, $CDCl_3$): δ 158.7, 158.5, 148.5, 141.9, 141.3, 140.6, 139.8, 131.7, 129.5, 129.2, 128.4, 127.0, 126.4, 125.6, 124.1, 123.6, 122.8, 120.4, 120.1, 117.7, 115.6, 114.1, 113.0, 110.2, 110.1, 80.6, 68.4, 31.9, 29.7, 29.6, 29.5, 29.4, 29.3, 29.2, 26.1, 22.7, 14.1; MS (FAB, 70 eV): m/z (relative intensity) 661 (M^+ , 100); HRMS calcd for $C_{44}H_{43}N_3OS$: 661.3121, found 663.3119.

2.3.12 2-((4-(5-(9-(4-(Dodecyloxy)phenyl)-9H-carbazol-3-yl)thiophen-2-yl)phenyl)-methylene)-2H-indene-1,3-dione (**F6**).

Compound **F6** was synthesized according to the same procedure as that of **F1**. Red solid of **F6** was obtained in 76% yield. MP: 176-178 °C. 1H NMR (500 MHz, $CDCl_3$): δ 8.48 (d, 2H, $J = 8.35$ Hz), 8.33 (d, 1H, $J = 1.04$ Hz), 8.14 (d, 1H, $J = 7.65$ Hz), 7.93-7.98 (m, 2H), 7.81 (s, 1H), 7.72-7.75 (m, 4H), 7.64 (dd, 2H, $J = 8.50, 1.45$ Hz), 7.46 (d, 1H, $J = 3.75$ Hz), 7.37-7.41 (m, 3H), 7.33 (d, 1H, $J = 3.80$ Hz), 7.25-7.30 (m, 3H), 7.07 (d, 2H, $J = 8.75$ Hz), 4.03 (t, 2H, $J = 6.50$ Hz), 1.81-1.84 (m, 2H), 1.45-1.50

(m, 2H), 1.22-1.38 (m, 16H), 0.86 (t, 3H, $J = 6.55$ Hz); ^{13}C NMR (125 MHz, CDCl_3): δ 190.5, 189.2, 158.6, 147.5, 146.1, 142.5, 141.9, 141.2, 141.0, 139.1, 135.3, 135.2, 135.0, 131.8, 129.6, 128.4, 128.3, 126.3, 126.2, 125.9, 125.1, 124.1, 123.6, 123.4, 123.2, 123.1, 122.9, 120.4, 120.0, 117.6, 115.6, 110.1, 110.0, 68.4, 31.9, 29.7, 29.6, 29.5, 29.4, 29.3, 29.2, 26.1, 22.7, 14.1. MS (FAB, 70 eV): m/z (relative intensity) 742 ($(\text{M}+\text{H})^+$, 100); HRMS calcd for $\text{C}_{50}\text{H}_{47}\text{NO}_3\text{S}$: 741.3272, found 742.3377.

2.3.13 (*E*)-2-(2-(*tert*-Butyl)-6-(4-(5-(9-(4-(dodecyloxy)phenyl)-9*H*-carbazol-3-yl)-thiophen-2-yl)styryl)-4*H*-pyran-4-ylidene)malononitrile (**F7**).

Compound **F7** was synthesized according to the same procedure as that of **F3**. The red solid of **F7** was collected in 60% yield (1.51 g, 2.23 mmol). MP: 145-147 °C. ^1H NMR (500 MHz, CDCl_3): δ 8.35 (s, 1H), 8.15 (d, 1H, $J = 7.70$ Hz), 7.65-7.68 (m, 3H), 7.52 (d, 2H, $J = 8.2$ Hz), 7.38-7.42 (m, 4H), 7.27-7.35 (m, 5H), 7.09 (d, 2H, $J = 8.7$ Hz), 6.70 (d, 1H, $J = 15.95$ Hz), 6.66 (d, 1H, $J = 1.55$ Hz), 6.53 (d, 1H, $J = 1.65$ Hz), 4.04 (t, 2H, $J = 6.5$ Hz), 1.82-1.85 (m, 2H), 1.46-1.51 (m, 2H), 1.33 (s, 9H), 1.23-1.32 (m, 16H), 0.87 (t, 3H, $J = 6.5$ Hz); ^{13}C NMR (125 MHz, CDCl_3): δ 172.1, 158.8, 158.6, 156.5, 146.3, 141.9, 141.1, 141.0, 137.0, 136.4, 133.0, 129.6, 128.4, 128.3, 126.3, 125.9, 125.6, 125.1, 124.0, 123.6, 123.2, 122.9, 120.3, 120.0, 117.8, 117.4, 115.6, 115.2, 115.1, 110.1, 110.0, 107.1, 102.6, 68.4, 63.0, 59.6, 36.6, 31.9, 29.7, 29.6, 29.5, 29.4, 29.3, 29.2, 28.1, 26.0, 22.6, 14.1; MS (FAB, 70 eV): m/z (relative intensity) 809 (M^+ , 100); HRMS calcd for $\text{C}_{54}\text{H}_{55}\text{N}_3\text{O}_2\text{S}$: 809.4015, found 809.4033.

2.3.14 (*E*)-2-(2-(*tert*-Butyl)-6-(4-(5-(9-(4-(dodecyloxy)phenyl)-9*H*-carbazol-3-yl)-thiophen-2-yl)styryl)-4*H*-pyran-4-ylidene)-1*H*-indene-1,3(2*H*)-dione (**F8**).

Compound **F8** was synthesized according to the same procedure as that of **F3**. Orange solid of **F8** was obtained in 66% yield. MP: 176-178 °C. ^1H NMR (500 MHz,

CDCl₃): δ 8.44 (s, 1H), 8.41 (s, 1H), 8.35 (d, 1H), 8.16 (d, 1H, $J = 7.65$ Hz), 7.74 (dd, 2H, $J = 19.45, 4.55$ Hz), 7.65-7.67 (m, 3H), 7.52-7.58 (m, 4H), 7.27-7.43 (m, 9H), 7.10 (d, 2H, $J = 8.40$ Hz), 6.84 (dd, 1H, $J = 16.0, 5.4$ Hz), 4.05 (t, 1H, $J = 6.3$ Hz), 1.82-1.88 (m, 2H), 1.60-1.62 (m, 2H), 1.48-1.54 (m, 2H), 1.44 (s, 9H), 1.37-1.41 (m, 2H), 1.27-1.32 (m, 12H), 0.89 (t, 3H, $J = 6.95$ Hz); ¹³C NMR (125 MHz, CDCl₃): δ 192.9, 173.9, 160.9, 158.7, 149.3, 146.2, 142.0, 141.4, 141.2, 140.9, 140.8, 136.1, 135.6, 133.8, 133.3, 129.8, 128.5, 128.4, 126.4, 126.2, 125.8, 125.0, 124.2, 123.7, 123.3, 123.1, 121.5, 121.3, 120.5, 120.1, 119.7, 117.6, 115.7, 110.2, 110.1, 109.2, 108.8, 103.7, 68.5, 37.1, 32.0, 29.9, 29.8, 29.7, 29.6, 29.5, 29.4, 28.5, 26.2, 22.8. MS (FAB, 70 eV): m/z (relative intensity) 890 ((M+H)⁺, 100); HRMS calcd for C₆₀H₅₉NO₄S: 889.4165, found 890.4248.

2.4 Quantum Chemistry Computations

All organic dyes were optimized by using B3LYP/6-31G* hybrid functional. For excited states, the time-dependent density functional theory (TDDFT) and the B3LYP functional were used. All analyses were performed using the Q-Chem 3.0 software. The frontier orbital plots of the highest and lowest occupied molecular orbitals (hereafter abbreviated as HOMO and LUMO, respectively) were drawn using GaussView 04.

3. Results and Discussion

3.1 Synthesis

The synthesis was started with **1a** or **1b**, onto which a bromo-substituent was added by using a bromination reaction to yield **2**. Then a thiophene unit was added to **2** by a Stille coupling reaction yielding **3** [56]. The π -bridge length was further increased by inserting another phenyl unit through a Stille coupling reaction with 4-bromobenzaldehyde to yield **4**. The eight final products were obtained through

Knoevenagel condensation with malononitrile, 1,3-indandione, and pyran derivatives, which were used to build up the four kinds of acceptor unit [57]. The structures of all new compounds were characterised through spectroscopic data.

3.2 Thermal stability

Thermal stability is essential for organic donor materials because of the vacuum deposition process followed in the fabrication of the photovoltaic devices. The thermal property of **F**-series was investigated through TGA and is shown in Fig. 2 and Table 1. The **F1~F4** exhibited a good thermal stability with a decomposition temperature (T_d , 5% weight loss) at 384~406 °C under N_2 condition. The **F5~F8** with flexible long chain showed slightly low T_d at 317~405 °C.

3.3 Absorption spectra

The ultraviolet-visible absorption spectra of all p-type materials in THF solution and the thin film are shown in Fig. 3 and Fig. S15~16. The photochemical and electrochemical parameters are listed in Table 1. All p-type materials exhibit broad and strong absorption in the range of 320~575 nm. Absorption in the short-wavelength region, 325–350 nm, is attributed to localised π - π^* and n - π^* transitions, and that in the long-wavelength region, 447~472 nm, results from intramolecular charge-transfer transitions (ICT). Compared to **F1**, **F3**, **F5**, and **F7**, the ICT transitions of **F2**, **F4**, **F6**, and **F8** are more red-shifted with the 1,3-indandione or pyran-based 1,3-indandione acceptor moiety assuming that 1,3-indandione group possess a stronger electron-withdrawing ability than dicyanovinylene moiety. The solid state absorption of ICT band on thin film shows a red shift of approximately 10~24 nm with respect to those in THF solution, and it is supposed to be the result of intermolecular J-aggregation

on the surface of substance. The compound **F1** and **F5** displays large stoke shift of 151 nm and 153 nm, respectively.

3.4 Electrochemical Properties

The ionic potentials (IP) corresponding to the highest occupied molecular orbital (HOMO) level of the dyes were measured by photo-electron spectroscopy (AC-2 PESA) and are presented in Fig. 4 and S17. Apparently, the dipolar π -conjugation system in the **F**-series and the electron-withdrawing moiety can strongly influence electron delocalization and the oxidation potential. The structures containing dicyanovinylene moiety as electron-withdrawing group in **F1**, **F3**, **F5**, and **F7** shows larger IP energy level compared to that with 1,3-indandione moiety. This observation also agrees well with the theoretical result (Fig. S18). The IP of the dyes decreased in the order **F1**~**F5** > **F2**~**F6**, and **F3**~**F7** > **F4**~**F8**. The EA levels of the dyes were estimated from the HOMO levels and zero-zero band gaps at the intersection of absorption and emission spectra (Table 1). The compound **F2**, and **F6** shows a narrow HOMO-LUMO energy gap, which is consistent with the wide absorption range and higher red-shift of ICT absorption band in Figure 3. **F1** compound shows the highest IP energy level and the largest gap with the LUMO energy level of acceptor materials C_{60} and C_{70} , indicating the high V_{oc} value in OPV devices.

3.5 Computational analysis

The electronic characteristics of **F**-series donor materials were investigated using theoretical models. Full geometrical optimisations were performed by the B3LYP/6-31G* hybrid functional, which was implemented in Q-Chem 3.0 [58]. The optimised molecular geometry of **F**-series donor materials are shown in Fig. 5 and S19. Clearly, the bridge conformation of the adjacent phenyl rings and anchoring group is

nearly coplanar, but the orientation of the adjacent carbazole (or phenyl group) and thiophene ring is slightly twisted to 13°-29° because of steric hindrance. The slight distortion in the bridge does not seem to inhibit the resonance between the electron donor and electron acceptor moieties. As depicted in Fig. 5 and S18, the electron densities in the HOMOs are distributed mainly around the carbazole donor sites, and those in the LUMOs are distributed around the acceptor moieties. As a consequence, HOMO to LUMO transition contributes more than 98% of first singlet excited state (S1 state) in all **F**-series materials.

The bar chart in Fig. 4 shows that **F1** exhibits the highest HOMO energy level than the others. The trend **F1**≈**F5** > **F2**≈**F6**, and **F3**≈**F7** > **F4**≈**F8** is similar with computed result. This observation can also be verified by comparing the dipole moments. **F1** (12.7477 D) and **F5** (14.2723 D) shows a larger dipole moment than that of **F2** (4.7393 D) and **F6** (8.717 D) as shown in Table S1. This large dipole moment could result from strong electron donating moiety of dicyanovinylene in **F1**, **F3**, **F5**, and **F7**.

The donor material **F1** displays the highest HOMO energy level (-5.38 eV) and supposed to have the largest gap with the LUMO energy level of acceptor materials C₆₀ or C₇₀, which is supported by the experimental data from AC-2. We expect that **F1** should provide high V_{oc} value in the OPVs device which further could be verified straightforwardly through the photovoltaic performance of the device fabricated by thermal deposition in vacuum.

3.6 Photovoltaic performance of bulk-heterojunction organic photovoltaic cells

To understand the relationship between molecular properties and device performance, we have prepared the bulk-heterojunction OPVs based on **F**-series donor materials and C₆₀ or C₇₀ acceptor for comparison. To address the effect of V_{oc} , OPV devices fabricated with our proposed donor materials were measured under the 1-sun illuminance for the

electrical characterizations. The electrical characteristics of the organic photovoltaics with **F1-F4** are summarized in Table 2 and the current density versus voltage curves of such devices are shown in Fig. 6. It has been reported vastly by many research groups that several mechanisms could strongly influence the value of V_{oc} . For example, the energy difference between donor and acceptor [59], charge transfer state [60] or energy coupling [61] of donor/acceptor, organic/electrode's energy barrier [62], the built-in potential in OPV [63], and interfacial energy at organic/organic [64] or organic/electrode [65] have been studied thoroughly on the variation in V_{oc} . Concerning the intrinsic analysis of our proposed materials in previous section, we expect that **F1** has a suitable energy level of HOMO/LUMO to achieve a high V_{oc} in OPVs due to a big energy-gap between the donor's HOMO and acceptor's LUMO. The OPV performance of **F1** exhibits a V_{oc} of 1.01 V (in Table 2), which is obviously higher than that of **F2-F4** ones. To date, only few researchers have presented V_{oc} value exceeding 1 V for a vacuum-deposited bulk-heterojunction small molecule OPVs [66]. It is obvious that a donor material with high HOMO level could achieve the high V_{oc} resulting in a high device performance. On the other hand, **F4** exhibits a lower value of V_{oc} due to its low HOMO level compared with **F1-F3**. In general, such result is consistent with previous work in the field of variation of V_{oc} [67]. On the other hand, in this work we still observed that the **F3** was not fully followed with such concept to obtain the high V_{oc} . The possible reason is because the chemical structure of **F3** donor showed the bulky tert-butyl group in pyran moiety as compared to those F-series materials (Fig. S19). Accordingly, it is possible that the V_{oc} value of **F3:C₆₀** is much lower than that of **F1:C₆₀** device although the **F1** (5.59 eV) and **F3** (5.52 eV) exhibited very similar HOMO values measured by low-energy photoelectron spectrometer. To confirm this hypothesis, we have compared the surface morphologies of **F1:C₆₀** and **F3:C₆₀** thin films in Fig. S20. Thin film of **F3:C₆₀** with few monolayers exhibits a rough surface

morphology affected by their chemical structure, resulting in the OPV device with a lower Voc.

More recently, Wong group reported that an OPV device with novel donor-acceptor-acceptor type organic dye extended to near-IR absorption region achieved a high PCE of 5.81% [26]. This work also pointed out a key issue of common organic donor with absorption range limited to visible light resulting in the poor device performance. To address this issue, we have studied the effect of the mixture of subphthalocyanine as donor and C₇₀ as acceptor in OPV at different mixing ratio [68]. The experimental result demonstrated that the PCE of OPVs can be significantly improved from 1.8% to 6.0% using a high concentration of C₇₀ in active layer owing to sufficient extended absorption range. Since, C₇₀ shows a wide and strong spectral absorption compared to C₆₀ or other acceptors [69]. Therefore, the active layer (**F1**:C₇₀) of 40 or 80 nm with two mixing ratios of 1:1 and 1:4 could be employed to improve the device performance. The EQE results are shown in Figure 6b and 6d. Using C₇₀ as acceptor into our proposed active layer, it is obvious that the **F1** in OPV shows a wide absorption spectrum in the range of 500-700 nm in comparison to their C₆₀ counterparts. We also observed that the 80 nm thick **F1**:C₇₀ (1:4) in OPV exhibited the highest PCE of 4.93%, which is much better than that of **F2-F4**. This result indicates that the active layer with high concentration of C₇₀ shows a wide absorption range, which, in turn, may improve the device performance. Indeed, we also observed that the active layer of **F1**:C₇₀ with optimal ratio shows a good charge balance and improved efficiency of carrier collection (see Fig. S21). Therefore, this phenomenon may contribute to improve the fill factor (*FF*) and hence an increase in the short-circuit current density (*J_{sc}*). On the other hand, in our previous work we have studied the optical interference effect on the varied film thickness of OPVs, which may affect the device performance by optimizing the optical-field intensity in the active layer [69]. In order to understand the effect of

optical interference on our proposed OPV with various thicknesses, the details of EQE and IQE of **F1:C₇₀** were measured for comparison as shown in Fig. S22. It is obvious that various thicknesses of active layer influence the optical distribution in the OPV structure, which strongly change the feature of IQE. For example, when the 80 nm **F1:C₇₀** active layer is used, the IQE showed a wide absorption profile compared to 40 nm ones solely due to the optical interference effect. This study might explain why OPV with the 80 nm active layer exhibited a good device performance. In addition, the film morphology is also a key factor to determine the device performance. To confirm this intrinsic property, we measured the rms roughness of the films and are presented in Fig. 7 which shows that rms roughness of the film increases from 0.913 to 2.52 nm as the **C₇₀** content increases. In the EQE data (see Fig. 6d), our devices with active layer of 1:1 or 1:4 show the same value at wavelength of 450 nm nevertheless the different mixing ratios of **F1:C₇₀**. This result probably indicates that the effective phase separation might be generated in our active layer to provide a better carrier transportation pathways resulting in the improvement of J_{sc} in our proposed device.

In order to evaluate the effect of the energy level of carbazole-based donors on V_{oc} , we have prepared the **F5-F8** OPVs for comparison as shown in Fig. 8 and summarized all results in Table 3. Obviously, the trend of the values of V_{oc} is inconsistent with their HOMO/LUMO levels. For example, the **F6** showed the higher V_{oc} as compared with **F5** and **F7-F8**. However, we believe that the V_{oc} is strongly dependent on several factors related to the molecular interaction of **F6:C₆₀**. To confirm this argument, the AFM measurement was taken to investigate the morphology difference between the **F5:C₆₀** and **F6:C₆₀** thin films as shown in Fig. S23. As expected, the rms value of **F6:C₆₀** film is 0.48 nm and this film exhibits very smooth surface morphology compared to other **F**-series donors. In previous work, we have demonstrated that the smooth active layer could suppress leakage current or reverse saturation current of the device, resulting in

high V_{oc} [70]. Indeed, the high efficiency of **F6** OPV is possibly because the active layer provides greater charge collection efficiency and extends the absorption range. In contrast, we found that the **F8** showed a very poor device performance in our study. Such issue may be attributed to the effect of intrinsic structural character of longer conjugation system, which results in the high LUMO level of 3.08 eV. Note that this phenomenon is consistent with theoretical calculation in Fig. S19. To find the relationship between the device performance and energy level, few research groups already reported that the interfacial layers at donor/acceptor [71], i.e. HOMO-HOMO, LUMO-LUMO or HOMO-LUMO [72], could highly affect the charge separation efficiency in active layer, resulting in the change of the OPV's J_{sc} and V_{oc} . Thus, the poor performance of **F8** is due to an increase in the gap of LUMO-LUMO in this study. Although the detail experiments are needed to study the interfacial mechanism of donor/acceptor, in this work we have synthesized the F-series donors to understand the relationship between the molecular structure and device performance, implying that the different intermolecular interaction or intrinsic structure of F-series donors:fullerene is crucial for improving OPV device characteristics.

4. Conclusions

In summary, we have synthesized the **F**-series p-type materials adopting carbazole moiety as the electron-donating (D) group combined with thiophenyl and phenyl as π -bridge, and the dicyanovinyl substituted or indendionevinyl or pyran-based as electron-withdrawing group (A) to form a D- π -A molecule in order to demonstrate its application in high performance OPVs. The high V_{oc} value in the OPVs device is supported strongly by computational result. The donor material **F1** displays the highest HOMO energy level (-5.38 eV) and the largest gap with the LUMO energy level of acceptor materials C_{60} or C_{70} , which is consistent with the experimental data from AC-2.

Further, we verified the photovoltaic performance of the device fabricated by thermal deposition in vacuum. The optimal OPVs device fabricated with **F1**:C₇₀ (1:4) as the active layer under vacuum deposition technique shows V_{oc} of 1.02 V and PCE of 4.93%, respectively.

Acknowledgments

This work was financial supported by the Ministry of Science and Technology of Taiwan (MOST 103-2113-M-029-007-MY2, 105-2221-E-131-016, 105-2119-M-131-001, and 105-2218-E-131-003), Tunghai University and Academia Sinica are gratefully acknowledged. Special thanks to Professor C.-P. Hsu at the Institute of Chemistry Sinica of Taiwan for her assistance on quantum chemistry computations.

Appendix. Supplementary data

The ¹H and ¹³C NMR spectra of all compounds, absorption spectra and emission spectra in THF solution, the absorption spectra on the film, TDDFT calculated orbitals, low energy transitions, space-charge limited current, CV spectra, HOMO/LUMO level, AFM images, internal quantum efficiency and absorption spectra. Supplementary data associated with this article can be found in the online version, at doi: <http://dx.doi.org>.

References

- [1] J. Potočník, Renewable Energy Sources and the Realities of Setting an Energy Agenda, *Science* 315 (2007) 810-811.
- [2] R. F. Service, Is It Time to Shoot for the Sun? *Science* 309 (2005) 548-551.
- [3] G. Yu, J. Gao, J. C. Hummelen, F. Wudl, and A. J. Heeger, Polymer photovoltaic cells: enhanced efficiencies via a network of internal donor-acceptor heterojunctions, *Science* 270 (1995) 1789-1791.
- [4] P. Peumans, and S. R. Forrest, Very-high-efficiency double-heterostructure copper phthalocyanine/ C_{60} photovoltaic cells, *Appl. Phys. Lett.* 79 (2001) 126-128.
- [5] H. Spanggaard, and F. C. Krebs, A brief history of the development of organic and polymeric photovoltaics, *Solar Energy Materials and Solar Cells* 83 (2004) 125-146.
- [6] J. You, L. Dou, K. Yoshimura, T. Kato, K. Ohya, T. Moriarty, K. Emery, C.-C. Chen, J. Gao, G. Li, and Y. Yang, A polymer tandem solar cell with 10.6% power conversion efficiency, *Nature Communications* 4 (2013) 1466.
- [7] C.-C. Chen, W.-H. Chang, K. Yoshimura, K. Ohya, J. You, J. Gao, Z. Hong, and Y. Yang, An efficient triple-junction polymer solar cell having a power conversion efficiency exceeding 11%, *Adv. Mater.* 26 (2014) 5670-5677.
- [8] Z. Zheng, S. Zhang, M. Zhang, K. Zhao, L. Ye, Y. Chen, B. Yang, and J. Hou, Highly efficient tandem polymer solar cells with a photovoltaic response in the visible light range, *Adv. Mater.* 27 (2015) 1189-1194.
- [9] S.-W. Chiu, L.-Y. Lin, H.-W. Lin, Y.-H. Chen, Z.-Y. Huang, Y.-T. Lin, F. Lin, Y.-H. Liu, and K. T. Wong, A donor-acceptor-acceptor molecule for vacuum-processed organic solar cells with a power conversion efficiency of 6.4%, *Chem. Commun.* 48 (2012) 1857-1859.
- [10] Y.-H. Chen, L.-Y. Lin, C.-W. Lu, F. Lin, Z.-Y. Huang, H.-W. Lin, P.-H. Wang, Y.-H. Liu, K.-T. Wong, J. Wen, D. J. Miller, and S. B. Darling, Vacuum-deposited

- small-molecule organic solar cells with high power conversion efficiencies by judicious molecular design and device optimization, *J. Am. Chem. Soc.* 134 (2012) 13616-13623.
- [11] Y. Zou, J. Holst, Y. Zhang, and R. J. Holmes, 7.9% efficient vapor-deposited organic photovoltaic cells based on a simple bulk heterojunction, *J. Mater. Chem. A*, 2 (2014) 12397-12402.
- [12] A. W. Hains, and T. J. Marks, High-efficiency hole extraction/electron-blocking layer to replace poly(3,4-ethylenedioxythiophene):poly(styrene sulfonate) in bulk-heterojunction polymer solar cells, *Appl. Phys. Lett.* 92 (2008) 023504.
- [13] R. Pandey, and R. J. Holmes, Graded donor-acceptor heterojunctions for efficient organic photovoltaic cells, *Adv. Mater.* 22 (2010) 5301-5305.
- [14] X. Che, X. Xiao, J. D. Zimmerman, D. Fan, and S. R. Forrest, High-efficiency, vacuum-deposited, small-molecule organic tandem and triple-junction photovoltaic cells, *Adv. Energy Mater.* 4 (2014) 1400568.
- [15] K. Schulze, C. Uhrich, R. Schüppel, K. Leo, M. Pfeiffer, E. Brier, E. Reinold, and P. Bäuerle, Efficient vacuum-deposited organic solar cells based on a new low-bandgap oligothiophene and fullerene C₆₀, *Adv. Mater.* 18 (2006) 2872-2875.
- [16] C.-L. Chung, C.-Y. Chen, H.-W. Kang, H.-W. Lin, W.-L. Tsai, C.-C. Hsu, and K.-T. Wong, A-D-A type organic donors employing coplanar heterocyclic cores for efficient small molecule organic solar cells, *Organic Electronics*, 28 (2016) 229-238.
- [17] B. Kan, Q. Zhang, M. Li, X. Wan, W. Ni, G. Long, Y. Wang, X. Yang, H. Feng, and Y. Chen, Solution-processed organic solar cells based on dialkylthiol-substituted benzodithiophene unit with efficiency near 10%, *J. Am. Chem. Soc.* 136 (2014) 15529-15532.
- [18] J. Sim, H. Lee, K. Song, S. Biswas, A. Sharma, G. D. Sharma, and J. Ko, Solution

- processed bulk heterojunction solar cells based on A-D-A small molecules with a dihydroindolindole (DINI) central donor and different acceptor end groups, *J. Mater. Chem. C* 4 (2016) 3508-3516.
- [19] B. Kan, M. Li, Q. Zhang, F. Liu, X. Wan, Y. Wang, W. Ni, G. Long, X. Yang, H. Feng, Y. Zuo, M. Zhang, F. Huang, Y. Cao, T. P. Russell, and Y. Chen, *J. Am. Chem. Soc.* 137 (2015) 3886-3893.
- [20] A. Zitzler-Kunkel, M. R. Lenze, T. Schnier, K. Meerholz, and F. Würthner, Comparative studies on optical, redox, and photovoltaic properties of a series of D-A-D and analogous D-A chromophores. *Adv. Funct. Mater.* 24 (2014) 4645-4653.
- [21] Z. Li, Q. Dong, Y. Li, B. Xu, M. Deng, J. Pei, J. Zhang, F. Chen, S. Wen, Y. Gao, and W. Tian, Design and synthesis of solution processable small molecules towards high photovoltaic performance, *J. Mater. Chem.* 21 (2011) 2159-2168.
- [22] T. Aytun, L. Barreda, A. Ruiz-Carretero, J. A. Lehrman, and S. I. Stupp, Improving solar cell efficiency through hydrogen bonding: a method for tuning active layer morphology, *Chem. Mater.* 27 (2015) 1201-1209.
- [23] H. M. Ko, H. Choi, S. Paek, K. Kim, K. Song, J. K. Lee, and J. Ko, Molecular engineering of push-pull chromophore for efficient bulkheterojunction morphology in solution processed small molecule organic photovoltaics. *J. Mater. Chem.* 21 (2011) 7248-7253.
- [24] H. Bürckstümmer, E. V. Tulyakova, M. Deppisch, M. R. Lenze, N. M. Kronenberg, M. Gsänger, M. Stolte, K. Meerholz, and F. Würthner, Efficient solution-processed bulk heterojunction solar cells by antiparallel supramolecular arrangement of dipolar donor-acceptor dyes, *Angew. Chem.* 123 (2011) 11832-11836.
- [25] V. Steinmann, N. M. Kronenberg, M. R. Lenze, S. M. Graf, D. Hertel, K. Meerholz, H. Bürckstümmer, E. V. Tulyakova, and F. Würthner, Simple, Highly efficient

- vacuum-processed bulk heterojunction solar cells based on merocyanine dyes, *Adv. Energy Mater.* 1 (2011) 888-893.
- [26] L.-Y. Lin, Y.-H. Chen, Z.-Y. Huang, H.-W. Lin, S.-H. Chou, F. Lin, C.-W. Chen, Y.-H. Liu, and K.-T. Wong, A low-energy-gap organic dye for high-performance small-molecule organic solar cells, *J. Am. Chem. Soc.* 133 (2011) 15822-15825.
- [27] H.-I. Lu, C.-W. Lu, Y.-C. Lee, H.-W. Lin, L.-Y. Lin, F. Lin, J.-H. Chang, C.-I. Wu, and K.-T. Wong, New molecular donors with dithienopyrrole as the electron-donating group for efficient small-molecule organic solar cells, *Chem. Mater.* 26 (2014) 4361-4367.
- [28] S. Steinberger, A. Mishra, E. Reinold, J. Levichkov, C. Uhrich, M. Pfeiffer, and P. Bäuerle, Vacuum-processed small molecule solar cells based on terminal acceptor-substituted low-band gap oligothiophenes, *Chem. Commun.* 47 (2011) 1982-1984.
- [29] R. Fitzner, E. Reinold, A. Mishra, E. Mena-Osteritz, H. Ziehike, C. Körner, K. Leo, M. Riede, M. Weil, O. Tsaryova, A. Weiß, C. Uhrich, M. Pfeiffer, and P. Bäuerle, Dicyanovinyl-substituted oligothiophenes: structure-property relationships and application in vacuum-processed small molecule organic solar cells, *Adv. Funct. Mater.* 21 (2011) 897-910.
- [30] S. Uchida, J. Xue, B. P. Rand, and S. R. Forrest, Organic small molecule solar cells with a homogeneously mixed copper phthalocyanine: C₆₀ active layer, *Appl. Phys. Lett.* 84 (2004) 4218-4220.
- [31] K. L. Mutolo, E. I. Mayo, B. P. Rand, S. R. Forrest, and M. E. Thompson, Enhanced open-circuit voltage in subphthalocyanine/C₆₀ organic photovoltaic cells, *J. Am. Chem. Soc.* 128 (2006) 8108-8109.
- [32] X. Tong, B. E. Lassiter, and S. R. Forrest, Inverted organic photovoltaic cells with high open-circuit voltage, *Organic Electronics* 11 (2010) 705-709.

- [33] P. Sullivan, A. Duraud, I. Hancox, N. Beaumont, G. Mirri, J. H.R. Tucker, R. A. Hatton, M. Shipman, and T. S. Jones, Halogenated boron subphthalocyanines as light harvesting electron acceptors in organic photovoltaics, *Adv. Energy Mater.* 1 (2011) 352-355.
- [34] C.-F. Lin, S.-W. Liu, C.-C. Lee, J.-C. Hunag, W.-C. Su, T.-L. Chiu, C.-T. Chen, and J.-H. Lee, Open-circuit voltage and efficiency improvement of subphthalocyanine-based organic photovoltaic device through deposition rate control, *Solar Energy Materials and Solar Cells* 103 (2012) 69-75.
- [35] S. Wang, E. I. Mayo, M. D. Perez, L. Griffe, G. Wei, P. I. Djurovich, S. R. Forrest, and M. E. Thompson, High efficiency organic photovoltaic cells based on a vapor deposited squaraine donor, *Appl. Phys. Lett.* 94 (2009) 233304.
- [36] X. Xiao, G. Wei, S. Wang, J. D. Zimmerman, C. K. Renshaw, M. E. Thompson, and S. R. Forrest, Small-molecule photovoltaics based on functionalized squaraine donor blends, *Adv. Mater.* 24 (2012) 1956-1960.
- [37] G. Chen, H. Sasabe, Z. Wang, X.-F. Wang, Z. Hong, Y. Yang, and J. Kido, Co-evaporated bulk heterojunction solar cells with > 6.0% efficiency, *Adv. Mater.* 24 (2012) 2786-2773.
- [38] A. Cravino, P. Leriche, O. Alévêque, S. Roquet, and J. Roncali, Light-emitting organic solar cells based on a 3D conjugated system with internal charge transfer, *Adv. Mater.* 18 (2006) 3033-3037.
- [39] O. Alévêque, P. Leriche, N. Cocherel, P. Frère, A. Cravino, and J. Roncali, Star-shaped conjugated systems derived from dithiafulvenyl-derivatized triphenylamines as active materials for organic solar cells, *Solar Energy Materials and Solar Cells* 92 (2008) 1170-1174.
- [40] H. Kagetama, O. Ohishi, M. Tanaka, Y. Ohmori, and Y. Shirota, High-performance organic photovoltaic devices using a new amorphous molecular material with high

- hole drift mobility, Tris[4-(5-phenylthiophen-2-yl)phenyl]amine, *Adv. Funct. Mater.* 19 (2009) 3948-3955.
- [41] J. Kalowekamo, and E. Baker, Estimating the manufacturing cost of purely organic solar cells, *Solar Energy* 83 (2009) 1224-1231.
- [42] Z. He, C. Zhong, X. Huang, W.-Y. Wong, H. Wu, L. Chen, S. Su, and Y. Cao, Simultaneous enhancement of open-circuit voltage, short-circuit current density, and fill factor in polymer solar cells, *Adv. Mater.* 23 (2011) 4636-4643.
- [43] E. Bundgaard, and F. C. Krebs, Low band gap polymers for organic photovoltaics, *Solar Energy Materials and Solar Cells* 91 (2007) 954-985.
- [44] R. F. Bailey-Salzman, and B. P. Rand, Near-infrared sensitive small molecule organic photovoltaic cells based on chloroaluminum phthalocyanine, *Appl. Phys. Lett.* 91 (2007) 013508.
- [45] J. Dai, X. Jiang, H. Wang, and D. Yan, Organic photovoltaic cells with near infrared absorption spectrum, *Appl. Phys. Lett.* 91 (2007) 253503.
- [46] S. Heutz, G. Salvan, T. S. Jones, and D. R. T. Zahn, Effects of annealing on the properties of molecular thin film heterostructures, *Adv. Mater.* 15 (2003) 1109-1112.
- [47] F. Yang, M. Shtein, and S. R. Forrest, Controlled growth of a molecular bulk heterojunction photovoltaic cell, *Nature Materials* 4 (2005) 37-41.
- [48] D. Y. Kim, G. Sarasqueta, and F. So, SnPc:C₆₀ bulk heterojunction organic photovoltaic cells with MoO₃ interlayer, *Solar Energy Materials and Solar Cells* 93 (2009) 1452-1456.
- [49] Y. Zhou, J. Pei, Q. Dong, X. Sun, Y. Liu, and W. Tian, Donor-Acceptor Molecule as the Acceptor for Polymer-Based Bulk Heterojunction Solar Cells, *J. Phys. Chem. C* 113 (2009) 7882-7886.
- [50] G. D. Sharma, J. A. Mikroyannidis, S. S. Sharma, and K. R. Justin Thomas, Bulk

- heterojunction organic photovoltaic devices based on small molecules featuring pyrrole and carbazole and 2-(4-nitrophenyl)acrylonitrile acceptor segments as donor and fullerene derivatives as acceptor, *Dyes and Pigments* 94 (2012) 320-329.
- [51] P. Li, H. Tong, J. Ding, Z. Xie, and L. Wang, Small molecules based on 2,7-carbazole for efficient solution-processed organic solar cells, *J. Mater. Chem. A*, 1 (2013) 8805-8812.
- [52] P. Li, H. Tong, J. Liu, J. Ding, Z. Xie, and L. Wang, An A'-A-D-A-A' type small molecule based on 2,7-carbazole for solution-processed organic solar cells with high open-circuit voltage, *RSC. Adv.* 3 (2013) 23098-23104.
- [53] Y. Kim, C. E. Song, S.-J. Moon, and E. Lim, Effect of dye end groups in non-fullerene fluorene and carbazole-based small molecule acceptors on photovoltaic performance, *RSC. Adv.* 5 (2015) 62739-62746.
- [54] M. Li, W. Ni, H. Feng, X. Wan, Y. Liu, Y. Zuo, B. Kan, Q. Zhang, and Y. Chen, A low bandgap carbazole based small molecule for organic solar cells, *Organic Electronics* 24 (2015) 89-95.
- [55] S. -W. Liu, W. -C. Su, C. -C. Lee, C. -F. Lin, C. -W. Cheng, C. -C. Chou, J. -H. Lee, and C. -T. Chen, Enhancement in open circuit voltage of organic photovoltaic devices through control of deposition rate of donor material, *Sol. Energy Mater. Sol. Cell.* 109 (2013) 280-287.
- [56] J. K. Stille, The palladium-catalyzed cross-coupling reactions of organotin reagents with organic electrophiles, *Angew. Chem. Int. Ed.* 25 (1986) 508-524.
- [57] E. Knoevenagel, Condensation von malonsäure mit aromatischen aldehyden durch ammoniak und amine, *Ber. Dtsch. Chem. Ges.* 31 (1898) 2596-2619.
- [58] Y. Shao, L. F. Molnar, Y. Jung, J. Kussmann, C. Ochsenfeld, S. T. Brown, A. T. B. Gilbert, L. V. Slipchenko, S. V. Levchenko, D. P. O'Neill, R. A. Jr. DiStasio, R. C. Lochan, T. Wang, G. J. O. Beran, N. A. Besley, J. M. Herbert, C. Y. Lin, T. V.

- Voorhis, S. H. Chien, A. Sodt, R. P. Steele, V. A. Rassolov, P. E. Maslen, P. P. Korambath, R. D. Adamson, B. Austin, J. Baker, E. F. C. Byrd, H. Dachsel, R. J. Doerksen, A. Dreuw, B. D. Dunietz, A. D. Dutoi, T. R. Furlani, S. R. Gwaltney, A. Heyden, S. Hirata, C.-P. Hsu, G. Kedziora, R. Z. Khalliulin, P. Klunzinger, A. M. Lee, M. S. Lee, W. Z. Liang, I. Lotan, N. Nair, B. Peters, E. I. Proynov, P. A. Pieniazek, Y. M. Rhee, J. Ritchie, E. Rosta, C. D. Sherrill, A. C. Simmonett, J. E. Subotnik, H. L., III Woodcock, W. Zhang, A. T. Bell, A. K. Chakraborty, *Advances in methods and algorithms in a modern quantum chemistry program package*, *Phys. Chem. Chem. Phys.* 8 (2006) 3172-3191.
- [59] M. Zhang, H. Wang, and C. W. Tang, Effect of the highest occupied molecular orbital energy level offset on organic heterojunction photovoltaic cells, *Appl. Phys. Lett.* 97 (2010) 143503.
- [60] C. -C. Lee, W. -C. Su, W. -C. Chang, B. -Y. Huang, and S. -W. Liu, The effect of charge transfer state on the open-circuit voltage of small-molecular organic photovoltaic devices: A comparison between the planar and bulk heterojunctions using electroluminescence characterization, *Org. Electron.* 16 (2015) 1-8.
- [61] P. Erwin, and M. E. Thompson, Elucidating the interplay between dark current coupling and open circuit voltage in organic photovoltaics, *Appl. Phys. Lett.* 98 (2011) 223305.
- [62] E. L. Ratcliff, A. Garcia, S. A. Paniagua, S. R. Cowan, A. J. Giordano, D. S. Ginley, S. R. Marder, J. J. Berry, and D. C. Olson, Investigating the influence of interfacial contact properties on open circuit voltages in organic photovoltaic performance: work function versus selectivity, *Adv. Energy Mater.* 3 (2013) 647-656.
- [63] B. Yang, F. Guo, Y. Yuan, Z. Xiao, Y. Lu, Q. Dong, and J. Huang, Solution-processed fullerene-based organic schottky junction devices for large-open-circuit-voltage organic solar cells, *Adv. Mater.* 25 (2013) 572-577.

- [64] A. Wilke, J. Endres, U. Hörmann, J. Niederhausen, R. Schlesinger, J. Frisch, P. Amsalem, J. Wagner, J. Gruber, A. Opitz, A. Vollmer, W. Brütting, A. Kahn, and N. Koch, Correlation between interface energetics and open circuit voltage in organic photovoltaic cells, *Appl. Phys. Lett.* 101 (2012) 233301.
- [65] C. -F. Lin, V. M. Nichols, Y. -C. Cheng, C. J. Bardeen, M. -K. Wei, S. -W. Liu, C. -C. Lee, W. -C. Su, T. -L. Chiu, H. -C. Han, L. -C. Chen, C. -T. Chen, and J. -H. Lee, Chloroboron subphthalocyanine/C60 planar heterojunction organic solar cell with N,N-dicarbazoyl-3,5-benzene blocking layer, *Sol. Energy Mater. Sol. Cell.* 122 (2014) 264-270.
- [66] S. -W. Liu, C. -F. Lin, C. -C. Lee, W. -C. Su, C. -T. Chen, and J. -H. Lee, High Open-Circuit Voltage Planar Heterojunction Organic Photovoltaics Exhibiting Red Electroluminescence, *J. Electrochem. Soc.* 159 (2012) H191-H194.
- [67] S. -W. Liu, and C. -F. Lin, Improvement in the open-circuit voltage of an organic photovoltaic device through selection of a suitable and low-lying highest occupied molecular orbital for the electron donor layer, *J. Mater. Res.* 28 (2013) 1442-1448.
- [68] S. -W. Liu, W. -C. Su, C. -C. Lee, C. -W. Cheng, C. -C. Chou, and C. -F. Lin, Absorbing visible light materials of Subphthalocyanine and C₇₀ for efficient planar-mixed organic photovoltaic devices, *J. Electrochem. Soc.* 160 (2013) G14-G18.
- [69] Chih-Chien Lee, Wei-Cheng Su, Yi-Sheng Shu, Wen-Chang Chang, Bo-Yao Huang, Ya-Ze Lee, Tsung-Hao Su, Kuan-Ting Chen, and Shun-Wei Liu, Decoupling the optical and electrical properties of subphthalocyanine/C70 bi-layer organic photovoltaic devices: improved photocurrent while maintaining a high open-circuit voltage and fill factor, *RSC Adv.* 5 (2015) 5617-5626.
- [70] J. Sakai, T. Taima, T. yamanari, and K. Saito, Annealing effect in the sexithiophene: C₇₀ small molecule bulk heterojunction organic photovoltaic cells, *Sol. Energy Mater.*

Sol. Cell. 93 (2009) 1149-1153.

- [71] T. D. Heidel, D. Hochbaum, J. M. Sussman, V. Singh, M. E. Bahlke, I. Hiromi, J. Lee, and M. A. Baldo, Reducing recombination losses in planar organic photovoltaic cells using multiple step charge separation, *J. Appl. Phys.* 109 (2011) 104502 1-6.
- [72] J. L. Brédas, J. E. Norton, J. Cornil, V. Coropceanu, Molecular understanding of organic solar cells: the challenges, *Acc. Chem. Res.* 42 (2009) 1691-1699.

TABLES

Table 1 Photochemical and electrochemical parameters of donor materials.

Donor material	HOMO/LUMO ^[a] (eV)	Band gap ^[a]	f^a	$\lambda_{\max}(\text{sol})/$ $\lambda_{\max}(\text{film})$ (nm) ^[b]	Em ^b (nm)	T _d (□)	IP ^c (eV)	E_g^d (eV)	EA ^e (eV)
F1	-5.38/-2.79	2.59	0.8644	451/470	602	384.4	-5.59	2.33	-3.26
F2	-5.16/-2.52	2.64	1.0952	472/488	622	397.1	-5.40	2.24	-3.16
F3	-5.23/-2.61	2.62	1.2023	447/457	592	414.3	-5.52	2.37	-3.15
F4	-5.10/-2.39	2.71	1.5433	470/486	597	406.2	-5.36	2.33	-3.03
F5	-5.32/-2.77	2.55	0.8234	452/477	605	355.5	-5.56	2.32	-3.24
F6	-5.11/-2.50	2.61	1.0343	472/496	622	317.6	-5.47	2.24	-3.23
F7	-5.18/-2.59	2.59	1.1383	449/463	597	392.7	-5.50	2.37	-3.13
F8	-5.06/-2.37	2.69	1.5349	470/489	599	405.8	-5.42	2.34	-3.08

^a TDDFT/B3LYP calculated values. ^b Absorption and Emission are in THF. ^c IP of film obtained from photo-electron spectrum (AC-2 PES). ^d E_g calculated by the intersection of absorption and emission spectra. ^e EA calculated by IP - E_g .

Table 2 Photovoltaic parameters of Devices made **F1~F4** with **C₆₀** and **C₇₀** as active layer.

Active layer (weight ratio)	V_{oc} (V)	J_{sc} (mA·cm ⁻²)	FF (%)	PCE (%) ^c	R_s (Ω cm ²)	R_{SH} (k Ω cm ²)
F1:C₆₀ (1:1) ^a	1.01	5.03	48.82	2.48	11.33	0.83
F2:C₆₀ (1:1) ^a	0.97	5.13	43.55	2.17	5.99	0.73
F3:C₆₀ (1:1) ^a	0.92	5.0	45.48	2.09	5.02	0.57
F4:C₆₀ (1:1) ^a	0.86	4.32	38.18	1.42	5.0	0.47
F1:C₇₀ (1:1) ^a	0.99	7.09	51.21	3.6	0.61	5.6
F1:C₇₀ (1:1) ^b	0.98	9.03	52.56	4.65	0.53	7.52
F1:C₇₀ (1:4) ^a	1.0	9.37	50.01	4.69	0.4	6.09
F1:C₇₀ (1:4) ^b	1.02	9.61	51.28	4.93	0.36	5.73

Device with ITO/MoO₃ (15 nm) /Active layer/ BCP (7nm)/Ag (120 nm)

^a Active layer (40 nm). ^b Active layer (80 nm). ^c Performance of **OPVs** measured in a 4 mm² working area on an ITO (10 Ω /square) substrate under AM 1.5 condition.

Table 3 Photovoltaic parameters of Devices made **F5~F8** with **C₆₀** and **C₇₀** as active layer.

Active layer (weight ratio)	V_{oc} (V)	J_{sc} (mA·cm ⁻²)	FF (%)	PCE (%) ^c	R_s (Ω cm ²)	R_{SH} (k Ω cm ²)
F5:C₆₀ (1:1) ^a	0.77	3.98	43.06	1.32	9.74	0.57
F5:C₆₀ (1:1) ^b	0.83	4.53	37.4	1.41	11.16	0.37
F6:C₆₀ (1:1) ^a	0.95	6.25	37.35	2.22	14.52	0.34
F6:C₆₀ (1:1) ^b	0.88	1.83	30.87	0.5	20.39	0.66
F6:C₇₀ (1:1) ^a	0.9	3.81	33.58	1.15	12.5	0.37
F6:C₇₀ (1:1) ^b	0.88	2.35	31.01	0.64	16.53	0.47
F7:C₆₀ (1:1) ^a	0.86	2.72	39.94	0.93	10.55	0.76
F7:C₆₀ (1:1) ^b	0.86	2.35	31.87	0.64	24.55	0.5
F8:C₆₀ (1:1) ^a	0.64	1.62	29.44	0.31	9.16	0.53
F8:C₆₀ (1:1) ^b	0.56	0.71	27.65	0.11	102.44	0.91

Device with ITO/MoO₃ (15 nm) /Active layer/ BCP (7nm)/Ag (120 nm)

^a Active layer (40 nm). ^b Active layer (80 nm). ^c Performance of **OPVs** measured in a 4 mm² working area on an ITO (40 Ω /square) substrate under AM 1.5 condition.

SCHEME CAPTIONS

Scheme 1. Synthesis route of **F**-series organic dyes. i) NBS, CH₂Cl₂; ii) 2-(Tributylstannyl)thiophene, PdCl₂(PPh₃)₂, DMF, 90 °C; iii) a. n-BuLi / (n-C₄H₉)₃SnCl, THF, -78 °C; b. 4-Bromobenzaldehyde, PdCl₂(PPh₃)₂, DMF, 90 °C; iv) Malononitrile or 1,3-Indandione or 2-(2-(*tert*-butyl)-6-methyl-4H-pyran-4-ylidene)malononitrile or 2-(2-(*tert*-butyl)-6-methyl-4H-pyran-4-ylidene)-1H-indene-1,3(2H)-dione, CH₃COONH₄, THF, reflux/ Piperidine, ACN, 90 °C.

FIGURE CAPTIONS

Fig. 1. Organic dye structures of **F**-series for OPVs p-type materials.

Fig. 2. Thermogravimetric analysis of **F**-series with a heating rate 10 °C min⁻¹ under N₂.

Fig. 3. Normalized absorption spectra of dyes in THF solution.

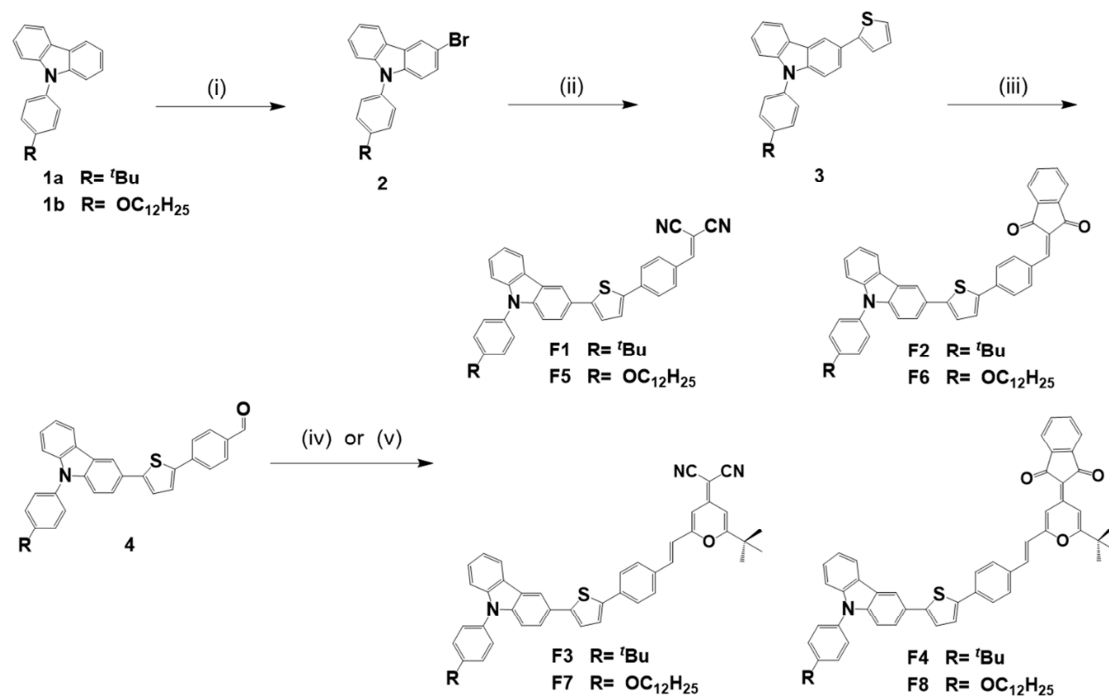
Fig. 4. Energy levels of **F**-series donor materials and other materials by AC-2 PESA use in small molecule OPVs.

Fig. 5. Computed optimum structure and frontier molecular orbitals of **F**-series calculated with TDDFT (B3LYP/6-31G*) in vacuum.

Fig. 6. *J-V* curves and EQE of the OPVs of **F1~F4** with C₆₀ and C₇₀. Note that the absorption spectrum of C₆₀ or C₇₀ was used for comparison.

Fig. 7. Atomic force microscopy images of 80 nm, (a) F1:C₇₀ of 1:1 and (b) F1:C₇₀ of 1:4.

Fig. 8. *J-V* curves and EQE of the OPVs of **F5~F8** with C₆₀. Note that the absorption spectrum of C₆₀ was used for comparison.



Scheme 1

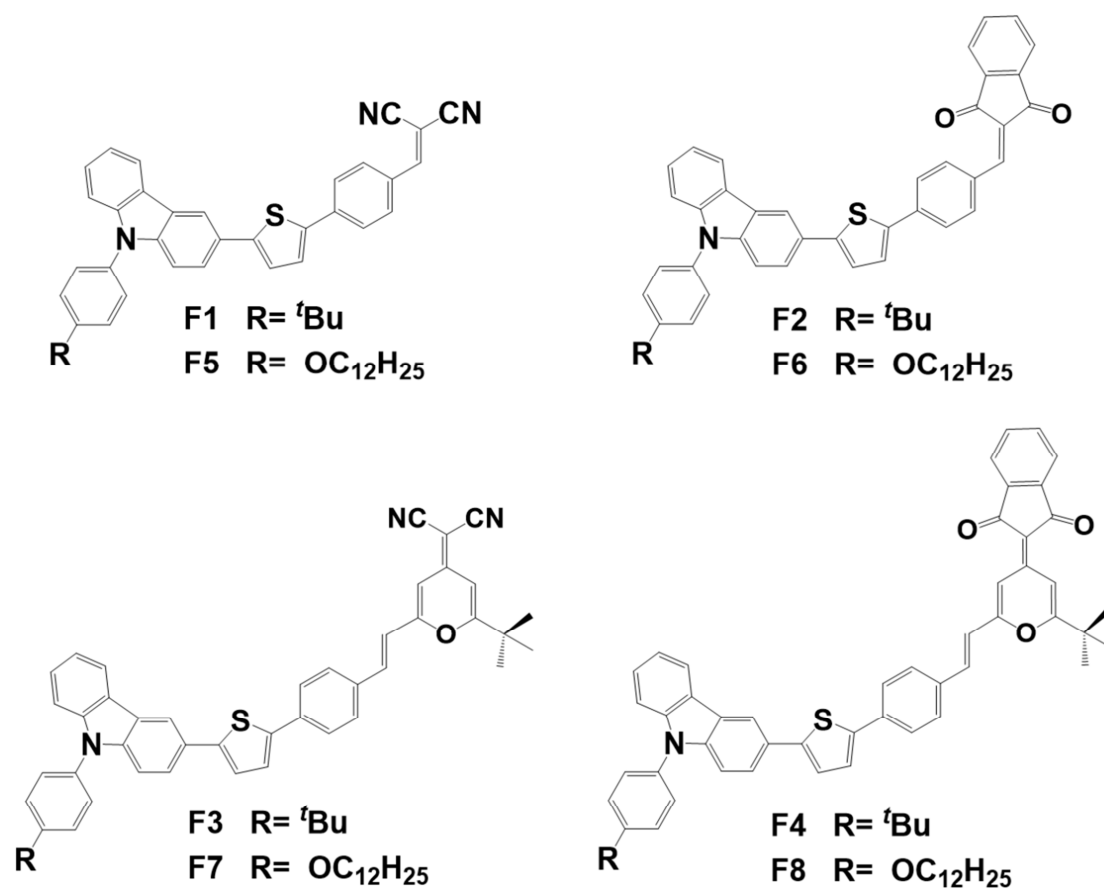


Figure 1

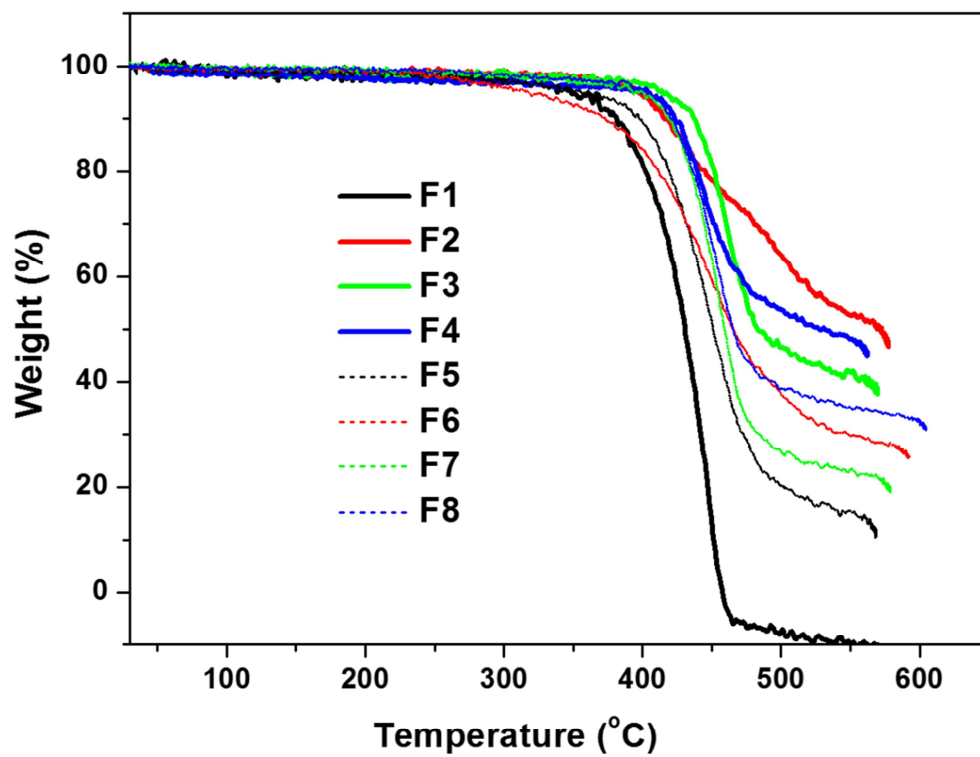


Figure 2

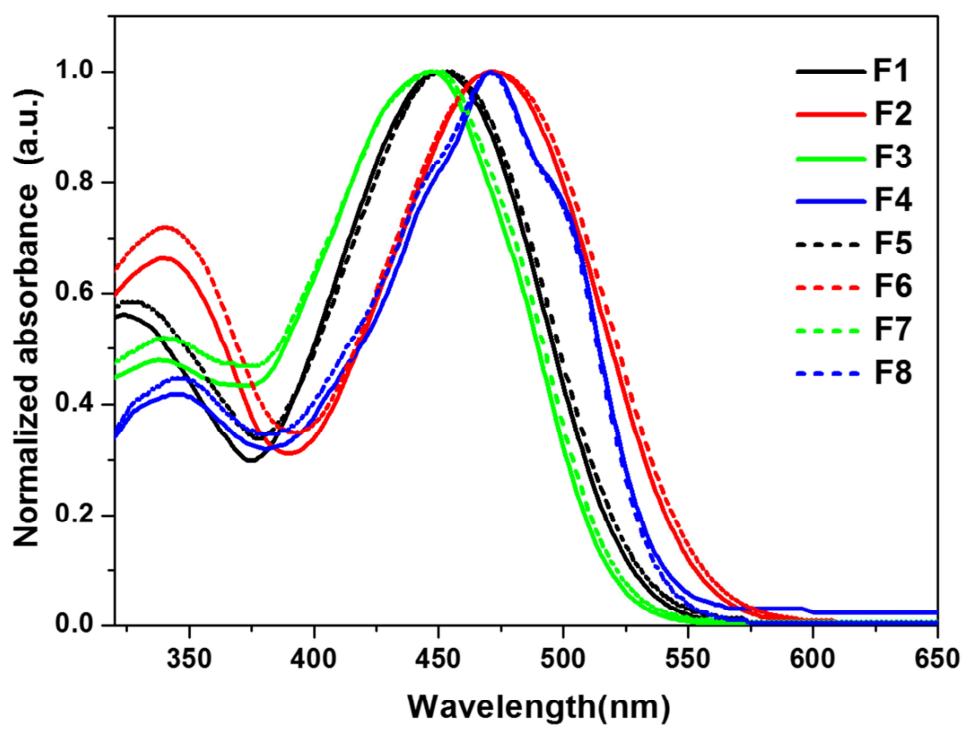


Figure 3

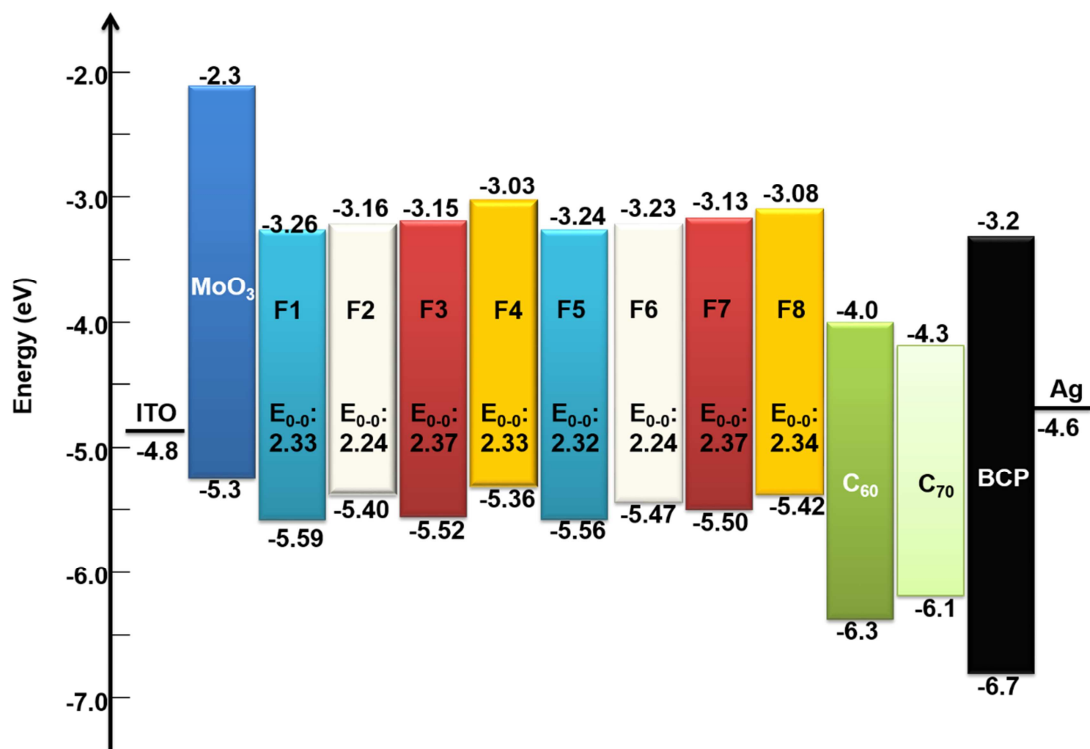


Figure 4

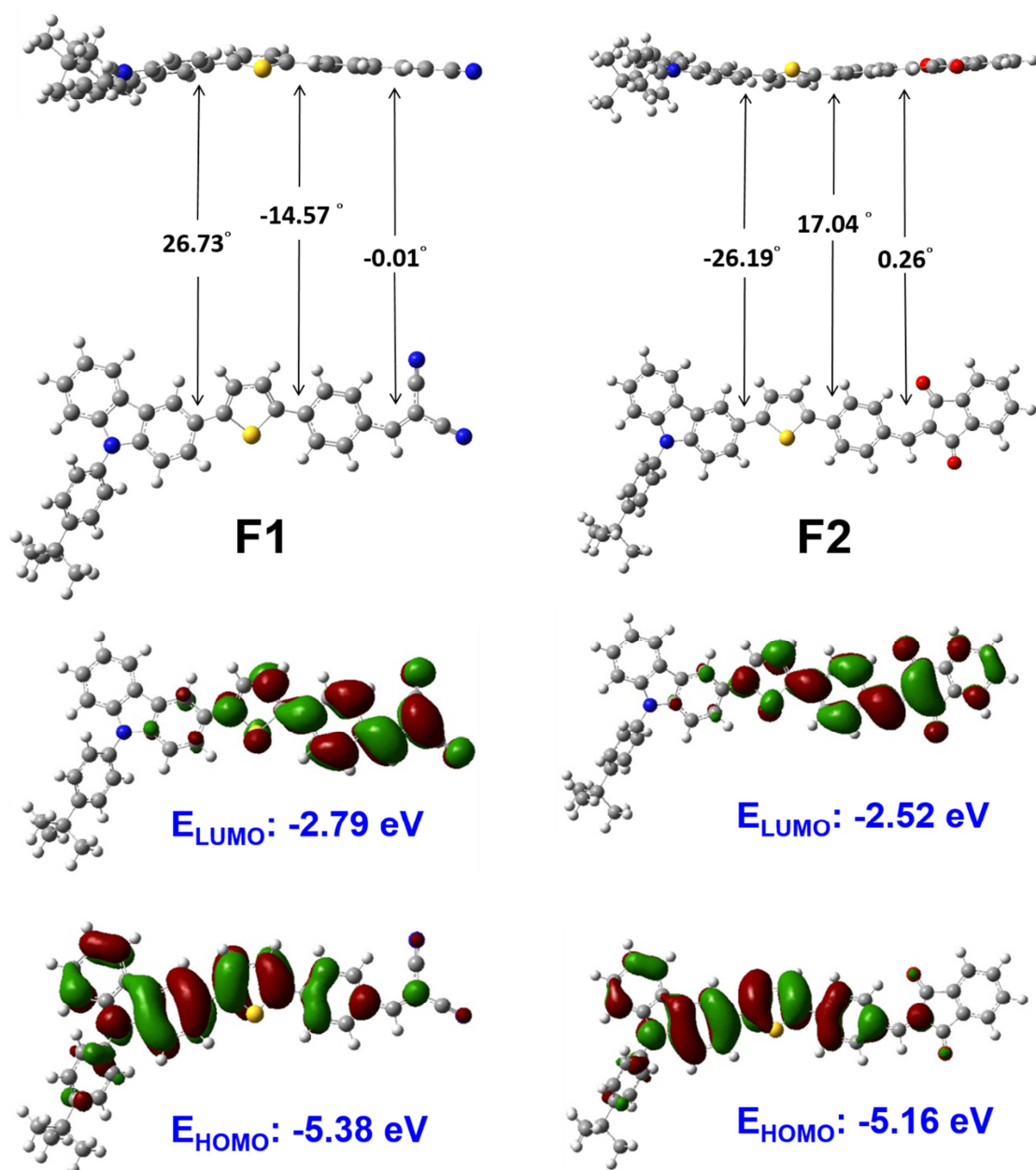


Figure 5

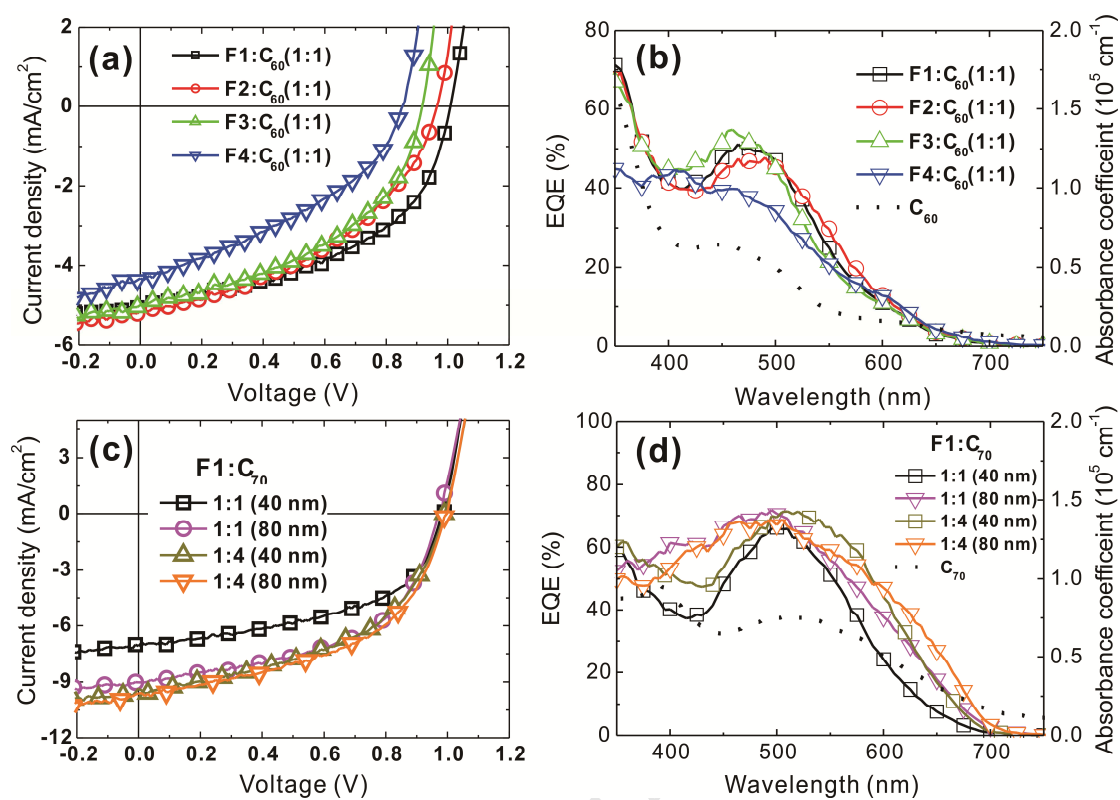


Figure 6

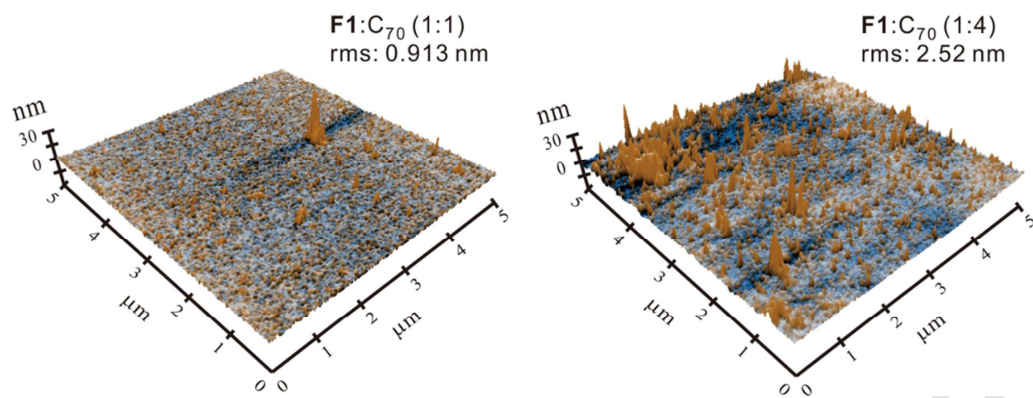


Figure 7

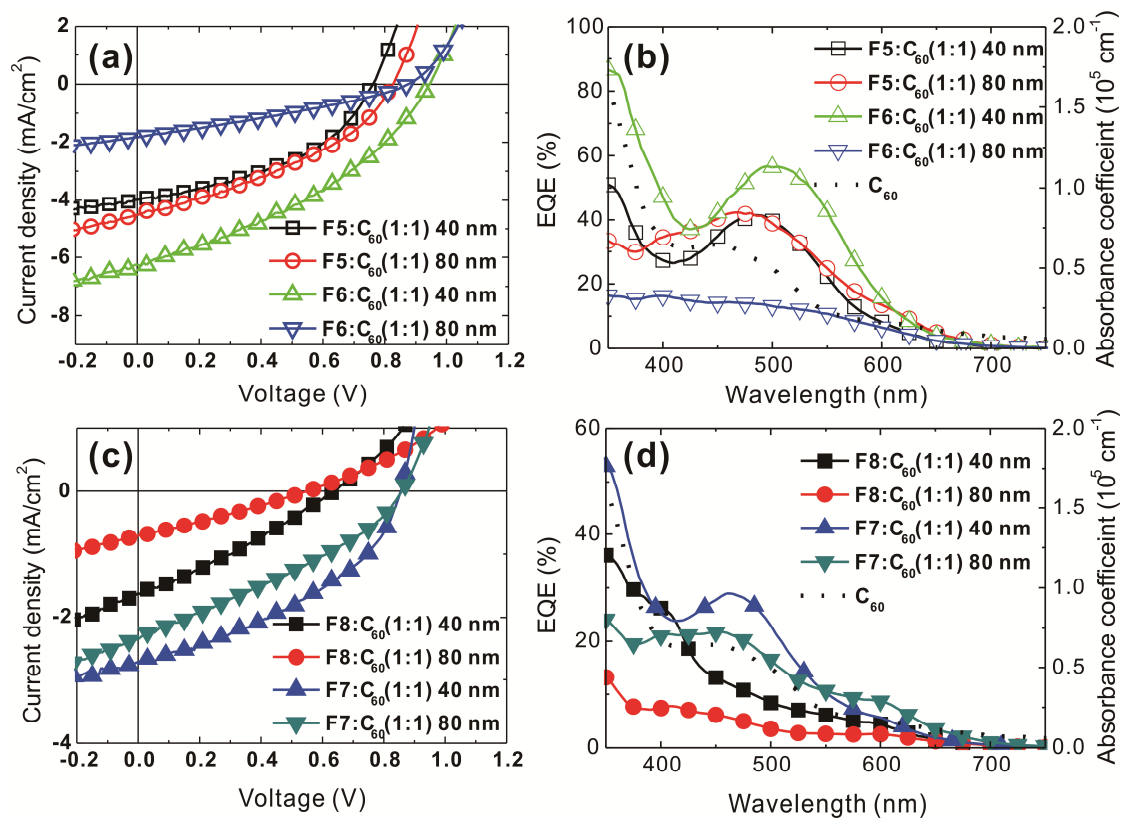


Figure 8

Highlights

1. Carbazole-based organic photovoltaic device exhibited the open-circuit voltage exceeding 1 V.
2. The p-type donor's structure was used the carbazole-based donor- π bridge-acceptor (D- π -A).
3. The active layer of F1:C₇₀ showed the good charge balance and small morphology.
4. The device with F1:C₇₀ exhibited a high power conversion efficiency of 4.93%.